Origin and provenance of spherules and magnetic grains at the Younger Dryas boundary

Yingzhe Wu[a,1], Mukul Sharma[a,2], Malcolm A. LeCompte[b], Mark N. Demitroff[c], and Joshua D. Landis[a]

[a]Radiogenic Isotope Geochemistry Laboratory, Department of Earth Sciences, Dartmouth College, Hanover, NH 03755; [b]Center of Excellence in Remote Sensing Education and Research, Elizabeth City State University, Elizabeth City, NC 27909; and [c]Department of Geography, University of Delaware, Newark, DE 19716

Edited* by Steven M. Stanley, University of Hawaii, Honolulu, HI, and approved July 23, 2013 (received for review March 5, 2013)

One or more bolide impacts are hypothesized to have triggered the Younger Dryas cooling at ∼12.9 ka. In support of this hypothesis, varying peak abundances of magnetic grains with iridium and magnetic microspherules have been reported at the Younger Dryas boundary (YDB). We show that bulk sediment and/or magnetic grains/microspherules collected from the YDB sites in Arizona, Michigan, New Mexico, New Jersey, and Ohio have $^{187}Os/^{188}Os$ ratios ≥1.0, similar to average upper continental crust (= 1.3), indicating a terrestrial origin of osmium (Os) in these samples. In contrast, bulk sediments from YDB sites in Belgium and Pennsylvania exhibit $^{187}Os/^{188}Os$ ratios <<1.0 and at face value suggest mixing with extraterrestrial Os with $^{187}Os/^{188}Os$ of ∼0.13. However, the Os concentration in bulk sample and magnetic grains from Belgium is 2.8 pg/g and 15 pg/g, respectively, much lower than that in average upper continental crust (=31 pg/g), indicating no meteoritic contribution. The YDB site in Pennsylvania is remarkable in yielding 2- to 5-mm diameter spherules containing minerals such as suessite (Fe-Ni silicide) that form at temperatures in excess of 2000 °C. Gross texture, mineralogy, and age of the spherules appear consistent with their formation as ejecta from an impact 12.9 ka ago. The $^{187}Os/^{188}Os$ ratios of the spherules and their leachates are often low, but Os in these objects is likely terrestrially derived. The rare earth element patterns and Sr and Nd isotopes of the spherules indicate that their source lies in 1.5-Ga Quebecia terrain in the Grenville Province of northeastern North America.

cometary | glaciation

The Younger Dryas (YD) event represents a major cooling interlude during the last deglaciation between 12.9 and 11.6 ka and is widely recorded over the mid- to high latitudes in the Northern Hemisphere with associated perturbations in the tropical regions. The abrupt onset of this event appears to have coincided with the Pleistocene megafaunal extinction in North America and Europe (1) and Clovis Paleoindian cultural modifications and population declines (2, 3). The prevalent postulated mechanism for the YD cooling is meltwater flooding and iceberg calving that released fresh water into the northeast Atlantic and/or the Arctic Oceans (4–7), resulting in a temporary shutdown of meridional overturning circulation (8). Recent modeling work (9) has added support to the idea that flooding of the Arctic via the McKenzie River could provide the "freshwater cap" that inhibited open-ocean deep convection.

Firestone et al. (10) proposed an alternate hypothesis that the cooling was directly or indirectly triggered by one or more cosmic airbursts or impacts that engendered enormous environmental and biotic changes. In support of this hypothesis, they reported extraterrestrial (ET) signatures from 12 sites dating to the Younger Dryas boundary (YDB) at ∼12.9 ka (10). The ET evidence from these sites is sometimes associated with a black layer (or black mat), which is also found at about 70 Clovis-age archaeological sites (1). Directly beneath the black mat is the YDB, a relatively thin layer, which is reported to exhibit variable enrichment in Ir (10). Firestone et al. (10) also found the YDB layer to be enriched in magnetic grains with variable amounts of Ir, magnetic microspherules, fullerenes containing ET ^{3}He, charcoal, soot, carbon spherules, and glass-like carbon. The impact hypothesis was further supported and extended by Kennett et al. (11), who reported nanodiamonds formed at high pressure at the YDB. The hypothesis is controversial, however, in part because other investigators have suggested alternate scenarios to explain the above evidential markers (12–15).

To date, 184 confirmed impact structures have been identified around the world (Earth Impact Database: www.passc.net/EarthImpactDatabase/index.html). Crater structure, shock metamorphism, and a meteoritic contribution are important markers used to confirm an impact structure (16–18). However, a visible crater, breccias, and high-pressure–modified minerals remain unreported for the YDB horizon, with the exception of possibly shock-synthesized hexagonal nanodiamonds (11, 19), an observation disputed by Daulton and coworkers (12, 15).

The proponents of the YDB impact hypothesis have pointed out, however, the lack of traditional impact markers in a number of widely accepted impact events (e.g., Australasian tektites, Libyan Desert glass, the Tunguska event), all suggested to have resulted from non-crater–producing airbursts (19, 20). Thus, a lack of traditional markers at the YDB may possibly be the result of one or more impactors exploding in the atmosphere or striking the Laurentide Ice Sheet (10). Recently, a submerged 4-km-wide candidate impact crater (Corossol Crater) has been discovered in the Sept Iles, Gulf of St. Lawrence, Canada and has been provisionally dated to 12.9 ka.[†] Two other features, one (Charity Shoal) submerged in Lake Ontario (21) and the other (Bloody Creek) in Nova Scotia (22), may represent additional or alternate impact craters associated with the YDB event. They have not been accurately dated, but their proposed range of dates spans the YD onset.

Significance

This study ties the spherules recovered in Pennsylvania and New Jersey to an impact in Quebec about 12,900 y ago at the onset of Younger Dryas. Our discovery resulted from an exhaustive search that examined the question of whether there is any evidence of extraterrestrial platinum group metals present in the bulk sediments, magnetic grains, and spherules recovered from the Younger Dryas boundary (YDB). We find that the spherules are likely quenched silicate melts produced following the impact at the YDB. The source of spherule osmium, however, is likely terrestrial and not meteorite derived.

Author contributions: Y.W. and M.S. designed research; Y.W., M.S., and J.D.L. performed research; M.A.L. and M.N.D. contributed samples; Y.W., M.S., and J.D.L. analyzed data; and Y.W., M.S., M.A.L., and M.N.D. wrote the paper.

The authors declare no conflict of interest.

*This Direct Submission article had a prearranged editor.

[1]Present address: Lamont–Doherty Earth Observatory, Columbia University, Palisades, NY 10964-8000.

[2]To whom correspondence should be addressed. E-mail: mukul.sharma@dartmouth.edu.

This article contains supporting information online at www.pnas.org/lookup/suppl/doi:10.1073/pnas.1304059110/-/DCSupplemental.

[†]Higgins MD, et al., Bathymetric and petrological evidence for a young (Pleistocene?) 4-km diameter impact crater in the Gulf of Saint Lawrence, Canada. Lunar and Planetary Science Conference XXXXII, March 7–11, 2011, abstr 1608.

A key piece of evidence reported by Firestone et al. (10) is that of anomalously high concentrations of magnetic spherules with diameters ranging from 10 to 150 μm and magnetic grains at the YDB. Magnetic grains at several YDB sites were reported to be enriched in Ir but inferred to show a nugget effect as sometimes Ir enrichment could not be reproduced (10). The concentrations of magnetic spherules reported by Firestone et al. (10) have been confirmed by seven independent groups (20, 23) from YDB sites in Venezuela (24), Arizona (25), New Mexico, South Carolina, and Maryland (26). Another study by Surovell et al. (27) was unable to replicate either the abundances or the chronostratigraphy of the magnetic spherules reported by Firestone et al. (10). That finding, however, has been contradicted by LeCompte et al. (26), who found magnetic spherules in three sites examined by Surovell et al. (27).

Studies investigating Ir enrichment in bulk sediment have also produced conflicting results. Paquay et al. (28) could not replicate the high values of Ir reported by Firestone et al. (10) at a number of locations, including Murray Springs, AZ. In contrast, Haynes et al. (29) found extremely high Ir concentrations in the YDB magnetic fraction (72 ng/g) at Murray Springs. This value is substantially higher than the 2.25 ng/g of Ir reported by Firestone et al. (10) in bulk sediment and is >3,000 times crustal abundance, exceeding concentrations found in most meteorites and impact craters. Similarly, anomalous enrichments in rare earth elements (REE) and high concentrations of both osmium (Os) and Ir in YDB sediments from Murray Springs and Lommel (Belgium) have been reported.[‡] Likewise, Ir enrichments in the YDB layer in southwest England have been reported.[§] Thus, some independent groups have confirmed YDB Ir anomalies, whereas others have not.

Although anomalously high concentrations of Ir are considered to be indicators of meteoritic influxes during an ET impact on Earth (30), high Ir concentrations alone are insufficient to prove an ET contribution as they can also result from terrestrial processes. Turekian (31) argued that Os concentrations and isotope measurements should be used to detect the existence of an ET component. Being a platinum group element (PGE), Os is highly enriched in meteorites/cosmic dust and depleted in the upper continental crust. The average Os/Ir ratios of meteorites and for the upper continental crust are 1.1 and 1.4, respectively (see compilation in ref. 32), implying little fractionation between these elements during continental crust formation. In contrast, the Os/Ir ratio in sediments is quite variable due to the differences in redox behavior of these elements. Thus, the Os/Ir ratio of organic rich black shale and pelagic carbonates (= 3–5) is much higher than that of Fe-Mn nodules/crusts and pelagic sediment (= 0.2–0.4) (32).

A difference in Os isotopic composition between meteorites and continental crustal rocks, however, makes Os isotopes a highly sensitive tracer of extraterrestrial material. Radiogenic ^{187}Os is produced from β-decay of ^{187}Re with a half-life of 42 Ga. The Os isotope ratio (^{187}Os with respect to stable and non-radiogenic isotope ^{188}Os) of various terrestrial and ET materials is thus a reflection of their Re/Os ratio and time elapsed after their formation from a primitive source. On average, $^{187}Os/^{188}Os$ ratios of meteorites/cosmic dust range from 0.117 to 0.128 and are similar to the primitive upper mantle (0.129 with $^{187}Re/^{188}Os$ = 0.36). In comparison, average $^{187}Os/^{188}Os$ ratio of the upper continental crust is approximately 10 times higher (1.26 with $^{187}Re/^{188}Os$ = 48). The Os concentration of meteorites is variable with ordinary and carbonaceous meteorites and cosmic dust ranging from 0.6 to 1 μg/g and iron meteorites ~30 μg/g (see compilation in ref. 32). In comparison, the Os concentration of terrestrial samples is from 3 ng/g (mantle peridotite) to 10–50 pg/g (loess samples representing average upper continental crust). Low $^{187}Os/^{188}Os$ ratio and high Os concentration in ET material provide a substantial contrast to the upper continental material with high $^{187}Os/^{188}Os$ ratio and extremely low Os concentrations. Thus, $^{187}Os/^{188}Os$ ratios combined with Os concentrations are a robust analytical approach to determine ET contribution in samples. A number of investigations have used Os isotope composition to trace meteorite impacts throughout geological time and to determine the extent to which the meteorite component is present in target rocks or in distal ejecta (e.g., tektites) from the impact (ref. 32 and references therein).

Paquay et al. (28) and others[¶] reported relatively high $^{187}Os/^{188}Os$ ratios in the bulk YDB sediments and concluded that PGEs in the YDB horizons in North America and Europe have a terrestrial origin. However, Firestone et al. (10) reported the highest Ir concentrations not in bulk sediments, but rather in the YDB magnetic grains. Moreover, they suggested that the magnetic grains and microspherules recovered from the YDB were most likely ET-impact ejecta. Because microspherules and magnetic grains constitute only a small fraction of YDB sediments (tens to hundreds of thousands of magnetic grains amounting to a few grams per kilogram; e.g., refs. 10, 23, 26), bulk sediment analyses can be expected to overwhelm Ir and Os values imparted by these materials. Consequently, it is essential to determine the Os abundance and isotope composition of magnetic spherules and grains to evaluate the origin and provenance of these objects.

Here we examine Os abundance and isotope ratios in YDB bulk sediment samples from six locations, including Blackwater Draw, NM; Sheriden Cave, OH; Murray Springs, AZ; Gainey, MI; Melrose, PA; and Lommel, Belgium. We also investigate magnetic grains for the Gainey and Lommel sites and magnetic microspherule clusters from Newtonville, NJ and Melrose, PA. Finally, we examine the origin and provenance of large (2- to 5-mm diameter) spherules from Melrose, using their mineralogy, major element, and REE contents and Os, Nd, and Sr isotope composition. Initial data from this study have been reported previously (¶, 33). For comparing results from other studies where only Ir is measured, we assume that ET Ir and Os should follow each other with an Os/Ir ratio of 1.1 as fractionation between Os and Ir during an impact is unlikely.

Results

Bulk Sediment Osmium Abundances. We investigated bulk sediment from five sites that were also examined by Firestone et al. (10) and/or Bunch et al. (20): Blackwater Draw, Sheriden Cave, Murray Springs, Gainey, and Lommel. These five sites all have reasonably robust chronostratigraphic control for the YDB. A bulk sediment sample containing magnetic grains and spherules from one other site in Melrose, PA was also examined. Chronostratigraphic control at Melrose is limited. A single optically stimulated luminescence (OSL) date was obtained for the colluvium above fragipan at the Melrose site, dating the bottommost part of the colluvium layer to ~16.4 ± 1.6 ka. This date was used by Bunch et al. (20) to estimate the YDB horizon at Melrose (Fig. S1).

Bulk sediment from six YDB sites exhibits Os concentration (= [Os]) ranging from 2.8 pg/g to 194 pg/g (Table 1). Four of these sites (Sheriden Cave, Murray Springs, Gainey, and Melrose) display [Os] similar to that of the upper continental crust. In comparison, the [Os] at Lommel is much lower than the typical crustal abundance. The Lommel YDB layer is a charcoal-rich quartz sand (10) and as quartz is not expected to be enriched in Os, the bulk [Os] appears to be consistent with the lithology.

[‡]Andronikov AV, Lauretta DS, Andronikva IE, Maxwell RJ, On the possibility of a Late Pleistocene, extraterrestrial impact: LA-ICP-MS analysis of the Black Mat and Usselo Horizon samples. 74th Meteoritical Society Meeting, August 8–12, 2011, abstr.

[§]Marshall W, Head K, Clough R, Fisher A., Exceptional iridium concentrations found at the Allerød-Younger Dryas transition in sediments from Bodmin Moor in southwest England. XVIII INQUA-Congress, July 21–27, 2011, abstr 2641.

[¶]Wu Y, Wilkes E, Kennett J, West A, Sharma M, The platinum group metals in Younger Dryas Horizons are terrestrial. American Geophysical Union, Fall Meeting, December 16, 2009, abstr PP31D-1389.

Firestone et al. (10) reported that the YDB at the Lommel site is enriched in magnetic grains, which have a concentration of 0.75 g/kg. They found that Ir concentration in bulk sediment was below the detection limit (<100 pg/g). However, they reported high concentrations of Ir in magnetic grains recovered from the Lommel site that were quite variable and ranged from 0.5 ng/g to 117 ng/g. Assuming all magnetic grains carry the same amount of Ir and there is no other phase carrying Ir in the Lommel sample, the expected amount of Ir in the sample is from 0.38 pg/g to 88 pg/g. Assuming that all Ir in the Lommel sample is meteorite derived, the expected [Os] in this sample would therefore be in a range of from 0.41 pg/g to 96 pg/g. The Lommel bulk sediment [Os] of 2.8 pg/g is thus above the lower limit estimated from the Firestone et al. (10) Ir data.

The bulk sample composed of fine-grained fluvial or lacustrine sediment at Blackwater Draw (10) is enriched in Os by about a factor of 6 more than average continental crust. Firestone et al. (10) reported a magnetic grain concentration of 2.1 g/kg at the YDB at Blackwater Draw. The Ir concentrations of bulk sample and magnetic grains are again quite variable from repeated analyses of different aliquots of the samples. The bulk samples [Ir] = <0.1–2.2 ng/g and for magnetic grains [Ir] = <6–24 ng/g (10). If magnetic grains are the only source of Ir and Os, the range of inferred Os concentration in bulk sediment is from <14 pg/g to 55 pg/g. As the Os concentration in the sample is 194 pg/g, it would indicate additional input of Os from terrestrial sources. If there is ET Os in the Blackwater Draw sample, it would therefore be reflected in its Os isotope composition, which will be weighted by the respective Os contributions from the ET and terrestrial end members.

Bulk Sediment Osmium Isotope Ratios. The $^{187}Os/^{188}Os$ ratios of four of the six sites examined (Blackwater Draw, Sheriden Cave, Murray Springs, and Gainey) are highly radiogenic, ranging from 1.35 to 3.06 with little indication of an ET signal (Table 1). At Blackwater Draw we also examined samples across the boundary and found that the $^{187}Os/^{188}Os$ ratios remain constant over the YDB horizon and are similar to those expected for the upper continental crustal materials (~1.3). The $^{187}Os/^{188}Os$ ratios decrease somewhat across the YDB at Sheriden Cave but remain highly radiogenic, ranging from 3.06 (0.8 cm below the YDB) to 2.61 (2.5 cm above the YDB). Overall, the YDB sedimentary Os for these four sites is terrestrial in origin and does not exhibit any evidence of mixing with meteoritic Os.

In contrast to the above sites, YDB bulk sediment from Lommel is remarkable in displaying a $^{187}Os/^{188}Os$ ratio of 0.80,

Table 1. Os analyses for bulk sediments, magnetic grains, and spherules from YDB layers

Site	Average YDB offset: depth, cm	Sample weight*	[Os], pg/g	$(^{187}Os/^{188}Os)_m$	$(^{187}Os/^{188}Os)_c$[†]
Bulk samples					
Blackwater Draw, NM	28	1.99098	279 ± 23	1.35 ± 0.03	1.35 ± 0.03
	14	2.27880	371 ± 30	1.34 ± 0.03	1.35 ± 0.03
	−1.5	2.03023	194 ± 16	1.35 ± 0.03	1.35 ± 0.03
	−21	1.97997	254 ± 20	1.35 ± 0.03	1.35 ± 0.03
	−55	0.97773	42 ± 3	1.35 ± 0.03	1.35 ± 0.03
Sheriden Cave, OH	2.5	1.02116	22 ± 2	2.60 ± 0.05	2.61 ± 0.05
	2.3	1.01876	30 ± 2	2.65 ± 0.05	2.65 ± 0.05
	0.5	1.00579	20 ± 2	2.90 ± 0.06	2.91 ± 0.06
	−0.8	1.04023	21 ± 2	3.06 ± 0.06	3.06 ± 0.06
Murray Springs, AZ	−1.5	0.97081	45 ± 4	1.66 ± 0.03	1.66 ± 0.03
Gainey, MI		0.99681	10 ± 1	2.92 ± 0.06	2.93 ± 0.06
Lommel, Belgium	−4	1.08946	2.8 ± 0.4	0.80 ± 0.02	0.80 ± 0.02
Melrose, PA	0	0.99399	53 ± 6	0.42 ± 0.01	0.42 ± 0.01
Laacher See tefra		1.01951	16 ± 1	2.12 ± 0.04	2.12 ± 0.04
Magnetic grains					
Gainey magnetic grain		2,648	152 ± 12	50 ± 1	56 ± 1
Lommel magnetic grain cluster		77	15 ± 1	0.6 ± 0.1	0.9 ± 0.1
Spherules from Newtonville, NJ and Melrose, PA					
NJ spherule cluster[‡]		470	3,373 ± 2,864[§]	1.00 ± 0.02	1.00 ± 0.02
PA spherule cluster[‡]		293	1,339 ± 1,576[§]	1.08 ± 0.02	1.08 ± 0.02
Object 3[‡]		35,424	109 ± 14	0.34 ± 0.01	0.34 ± 0.01
Object 8[‡]		9,581	309 ± 26	0.64 ± 0.01	0.64 ± 0.01
Object 2 residue		41,428	106 ± 9	0.181 ± 0.004	0.180 ± 0.004
Object 2 leachate		32[¶]	43,407 ± 26,350[§,¶]	0.118 ± 0.002	0.117 ± 0.002
Object 4 residue		19,266	107 ± 10	0.275 ± 0.005	0.274 ± 0.005
Object 4 leachate		21[¶]	49,407 ± 14,035[§,¶]	0.121 ± 0.002	0.120 ± 0.002
Object 5 residue		59,000	126 ± 12	0.75 ± 0.02	0.75 ± 0.02
Object 5 leachate		108[¶]	19,474 ± 5,055[§,¶]	0.113 ± 0.002	0.113 ± 0.002
Object 11 residue		9,143	55 ± 7	0.171 ± 0.003	0.169 ± 0.003
Object 11 leachate		8[¶]	32,914 ± 2,699[¶]	0.116 ± 0.002	0.113 ± 0.002
Object 13 residue		7,875	86 ± 8	0.145 ± 0.003	0.143 ± 0.003
Object 13 leachate		9[¶]	42,442 ± 3,422[¶]	0.114 ± 0.002	0.112 ± 0.002

*Sample weight is in grams for the bulk samples and in micrograms for the magnetic grains and spherules.

[†]Blank-corrected ($^{187}Os/^{188}Os$) ratios. Total chemistry blanks were processed along with the sample. The bulk sediment samples were corrected for a blank of 30 fg with $^{187}Os/^{188}Os = 0.47$ ($n = 1$). The magnetic grains from Gainey and Lommel were corrected for a blank of 5.6 fg with $^{187}Os/^{188}Os = 0.51$ ($n = 6$). With the preparation of new reagents the blank was further reduced before processing of the magnetic spherules from Melrose and Newtonville, which were corrected for a blank of 2.2 fg with $^{187}Os/^{188}Os = 0.49$ ($n = 6$).

[‡]Chemical separation with no leaching procedure.

[§]Underspiked.

[¶]Estimated values (spherule weight difference between before and after leaching procedure).

Table 2. Sr, Nd, and Sm analyses for microspherule cluster from Pennsylvania and individual spherules from Melrose, PA

Site	Sample weight, μg	[Sr] ppm	$^{87}Sr/^{86}Sr$*	[Sm] ppm	[Nd] ppm	$f_{(Sm/Nd)}$†	ε_{Nd}	T_{DM}‡
PA spherule cluster§	293	75.2 ± 0.2	0.712449 ± 11	—	30.8 ± 0.3	—	−11.50 ± 2.92	—
Object 3§	35,424	123.0 ± 0.3	0.713495 ± 438	4.9 ± 0.2	26.3 ± 0.2	−0.41	−11.51 ± 0.17	1.55
Object 8§	9,581	603.2 ± 1.4	0.712586 ± 180	10.4 ± 0.3	51.9 ± 0.5	−0.39	−11.69 ± 0.52	1.63
Object 2 residue	41,428	768.3 ± 1.8	0.710965 ± 22	5.9 ± 0.2	28.8 ± 0.3	−0.37	−11.42 ± 0.30	1.68
Object 4 residue	19,266	450.5 ± 1.0	0.713673 ± 18	10.6 ± 0.3	51.4 ± 0.5	−0.36	−11.99 ± 0.41	1.77
Object 5 residue	59,000	199.7 ± 0.5	0.710794 ± 49	3.5 ± 0.1	19.9 ± 0.2	−0.46	−11.61 ± 0.61	1.42
Object 11 residue	9,143	470.7 ± 1.1	0.711493 ± 30	5.2 ± 0.2	27.3 ± 0.3	−0.40	−9.83 ± 0.49	1.44
Object 13 residue	7,875	308.1 ± 0.8	0.716196 ± 50	6.5 ± 0.2	33.2 ± 0.8	−0.40	−11.06 ± 0.24	1.54

*2σ uncertainty, ppm.
†$f_{(Sm/Nd)} = [(^{147}Sm/^{144}Nd)_{sample}/(^{147}Sm/^{144}Nd)_{CHUR} - 1]$, where $(^{147}Sm/^{144}Nd)_{CHUR} = 0.1967$.
‡T_{DM} is denoted depleted mantle model age, calculated by $\varepsilon_{Nd} = 0.25 \times T_{DM}^2 + (f_{(Sm/Nd)} \times Q - 3) \times T_{DM} + 8.5$, where $Q = 25.13$ Ga^{-1}.
§Chemical separation with no leaching procedure.

a value that is much lower than that of average upper continental crust. We considered whether the low $^{187}Os/^{188}Os$ ratio at Lommel might result from mixing with YD-age Laacher See volcanics.[||] Bulk analysis of Laacher See tuff ruled out this possibility, because its $^{187}Os/^{188}Os$ ratio is 2.12 (Table 1) and much higher than that at Lommel. So although the low $^{187}Os/^{188}Os$ ratio suggests contribution from an impactor, the low [Os] indicates no contribution from the impactor. This can be assessed using the following mass balance equation that relates the fraction of ET Os present (f_β) to the concentrations and isotopic compositions of the continental and ET end members and the resulting mixture,

$$f_\beta = \frac{C_{mix}R_{mix} - C_\alpha R_\alpha}{C_\beta R_\beta - C_\alpha R_\alpha},$$

where C and R refer to concentration and isotope composition, respectively, and subscripts α, β, and *mix* correspond to continental crust, meteorite, and resulting mixture, respectively. For $C_\alpha = 10$ pg/g and $R_\alpha = 1.3$ and $C_\beta = 0.6$ μg/g and $R_\beta = 0.126$, we find that $f_\beta = 0$. In the absence of significant enrichment in Os expected from mixing with ET Os two other explanations are possible: (*i*) our sample of the YDB horizon at Lommel did not pick up high Ir- (and Os)-bearing magnetic grains as their number density in the sediment is rather low ("nugget effect") (10) and (*ii*) the quartz sands at Lommel were derived from a source with time-integrated Re/Os ratio that is much lower than that of average continental crust.

The bulk sediment from the Melrose, PA site exhibits the lowest $^{187}Os/^{188}Os$ ratio (0.42) of all of the bulk samples analyzed, although its Os concentration (53 pg/g) is similar to terrestrial values. So although the low $^{187}Os/^{188}Os$ ratio suggests contribution from an impactor, the low [Os] indicates remarkably little PGE contribution from the impactor. This can be assessed using the mass balance equation given above. For $C_\alpha = 10$ pg/g and $R_\alpha = 1.3$ and $C_\beta = 0.6$ μg/g and $R_\beta = 0.126$, we find that $f_\beta = 0.01\%$. This calculation is very sensitive to the chosen value of C_β with f_β becoming 0 for $C_\beta \geq 17.1$ pg/g.

The above observations led us to investigate whether the magnetic grains recovered from a larger sample of YDB at Lommel might contain ET-sourced Os with $^{187}Os/^{188}Os$ ratios lower than those of the bulk sediment. In addition, we analyzed microspherule clusters and individual objects recovered from Melrose. A large single magnetic grain from YDB at Gainey, MI, where Firestone et al. (10) reported enrichment in magnetic spherules and a cluster of magnetic spherules recovered from YDB at Newtonville, NJ were also analyzed.

[||]Beets C, Sharma M, Kasse, K, Bohncke S, Search for extraterrestrial osmium at the Allerød-Younger Dryas boundary. American Geophysical Union, Fall Meeting, December 19, 2008, abstr V53A-2150.

Magnetic Grains. The Os analyses of a single large magnetic grain from Gainey and a cluster of magnetic grains from Lommel are given in Table 1. The Gainey magnetic grain is highly enriched in Os ([Os] = 152 pg/g) but has an extremely high $^{187}Os/^{188}Os$ ratio (= 56). Considering that the bulk sediment from Gainey has [Os] and $^{187}Os/^{188}Os$ ratio of 10 pg/g and 2.93, respectively, it is evident that the magnetic grain we analyzed is anomalous and it does not control the inventory of Os in the bulk sediment. In comparison, [Os] and $^{187}Os/^{188}Os$ ratio of the Lommel magnetic grain cluster are 15 pg/g and 0.9 ± 0.1, respectively. The Os isotope composition of the grain cluster is thus virtually identical to that of the bulk sediment from Lommel. If the Lommel sample contains 0.75 g/kg of magnetic grains (10), it implies that they contribute only a very small fraction of Os (0.01%) to the bulk sediment. These results indicate that Os (and other PGEs) in the magnetic grains and bulk rocks from Lommel and Gainey is likely not derived from an ET source. Alternately, we have missed the highly enriched magnetic grains analyzed by Firestone et al. (10) due to the nugget effect and grains extracted from a larger volume of YDB samples will be needed to capture these elusive grains.

Microspherule Clusters from Melrose, PA and Newtonville, NJ. Microspherules from Melrose and Newtonville are ~5–50 μm in diameter (Fig. S2). Their major element compositions were estimated using SEM-energy dispersive X-ray spectroscopy and were found to be dominated by Al, Si, and Fe. The microspherule clusters were analyzed for Os, Sr, Nd, and Sm, using a procedure that permits sequential separation of these elements from a given sample (Fig. S3). We measured the microspherules as clusters because individual microspherules are small and adhere to each other (Fig. S2). The Os, Sr, and Nd isotope data for the microspherules are shown in Tables 1 and 2. The [Os] of these objects is extremely high compared with the average crustal value but with high uncertainty. The $^{187}Os/^{188}Os$ ratios are ~1. The Sr isotope composition (Table 2) of the cluster of microspherules from Pennsylvania is radiogenic (= 0.7124). The Nd isotope composition of this cluster is nonradiogenic ($\varepsilon_{Nd} = -11.5$). The Sr and Nd isotope data indicate that the provenance of these spherules is most likely not meteoritic, but rather ancient upper crust (see below).

Individual Objects from Melrose, PA. Individual spherules from the YDB layer at Melrose range from 2 mm to 5 mm in diameter (Fig. 1). SEM images of these polished sections revealed the presence of a variety of high-temperature minerals and textures (Figs. 2–4), indicating melting followed by rapid cooling. The chemical compositions of the identified minerals are given in Tables S1 and S2 and their occurrence in individual spherules is listed in Table S3. The spherules exhibit skeletal crystals (i.e., crystals with cavities) with swallowtails, herringbone texture, and flow bands (schlieren) present in a background of glass. Lath-like mullite crystals are often present in some objects (Fig. 2 *A* and *D*), associated with other crystallites such as cordierite and

Ni-rich hercynite–magnetite displaying bright herringbone textures (Fig. 2 *B* and *C*). One spherule has high-temperature corundum crystals (Fig. 2*E*) and another exhibits flow structure in silica (lechatelierite, Fig. 2*F*). Iron is present as droplets in several forms: Fe metal, Fe oxide, Fe sulfide, suessite (Fe-Ni silicide), and schreibersite (Fe-Ni phosphide) (Fig. 3). Schreibersite is non-stoichiometric with 6.98% Ni (Table S2) in comparison with stoichiometric schreibersite (empirical formula = $Fe^{0+}_{2.25}Ni_{0.75}P$), which has Ni = 21.9 wt%. Most of the Fe droplets are Fe metal or Fe sulfide, which are enriched closer to the surface rather than in the inner part of the spherule (Fig. 4). Two spherules have an Fe oxide rim (Figs. 1*C* and 4).

The bulk chemical composition of two spherules and the composition of glass in five others (Tables S3 and S4) indicate that the spherules are enriched in SiO_2, Al_2O_3, and FeO. The relative proportions of Si, Al, and Fe in the bulk spherules are similar to those in North American Shale Composite (NASC) (34) (Fig. S4). The glass compositions of the spherules have SiO_2 contents between 42 wt% and 66 wt%; TiO_2 contents, 1–3 wt%; Al_2O_3 contents, 19–28 wt%; MgO contents, ∼1 wt%; CaO contents, 1–8 wt%; FeO contents, 3–20 wt%; Na_2O contents, ∼1 wt%; and K_2O contents, 1–5 wt%. Characteristically, all glasses show normative corundum. The mineral composition ranges are quartz, 12–41 wt%; corundum, 11–20 wt%; orthoclase, 2–29 wt%; albite, <0.1–9 wt%; anorthite, 2–16 wt%; hypersthene, 6–37 wt%; ilmenite, 2–5 wt%; and apatite, <1–8 wt%. The Melrose spherules can be divided into two categories on the basis of whether or not they contain reduced iron, including native iron, iron sulfides, phosphides, or silicides: (*i*) oxidized spherules (objects 1 and 12) containing low total alkalis ($K_2O + Na_2O < 2$ wt%) and (*ii*) reduced spherules objects (objects 6, 7, and 10) containing high amounts of total alkalis ($K_2O + Na_2O > 4$ wt%). Because objects 14 and 15 have no mineral data available, we use total alkali contents to assign them in the above categories (Fig. S5).

The spherules display a chondrite-normalized REE pattern that is characteristic of upper continental crust (Fig. S4) (35). The Sr isotope composition of these spherules is highly radiogenic, ranging from 0.711 to 0.716 (Table 2). The Nd isotope composition of the objects is highly nonradiogenic with ε_{Nd} ranging from −9.83 to −11.99 with Sm/Nd ratios of ∼0.11 ($f_{Sm/Nd}$ of −0.4). The depleted mantle model ages (T_{DM}, Table 2) for the spherules range from 1.42 to 1.78 Ga. The Sr and Nd isotopes

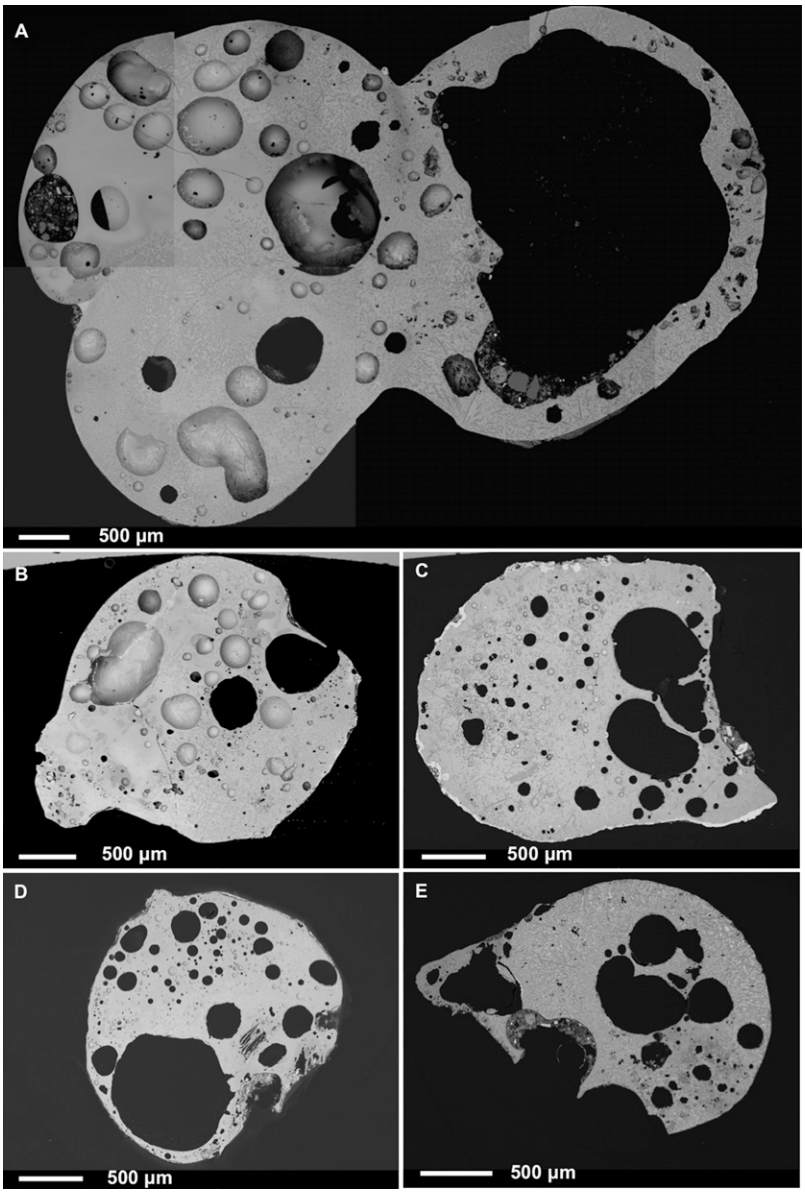

Fig. 1. Backscattered emission (BSE) images of polished sections of magnetic spherules from the inferred YDB layer in Melrose, PA. All objects appear to have large bubbles presumably filled with air or gas. (*A*) Object 1 is dumbbell shaped. (*B*) Object 6. (*C*) Object 7 has a rim enriched in Fe. (*D*) Object 10 has a small spherule welded to it. (*E*) Object 12 displays a tail. The picture for object 1 is a composite of several SEM-BSE images.

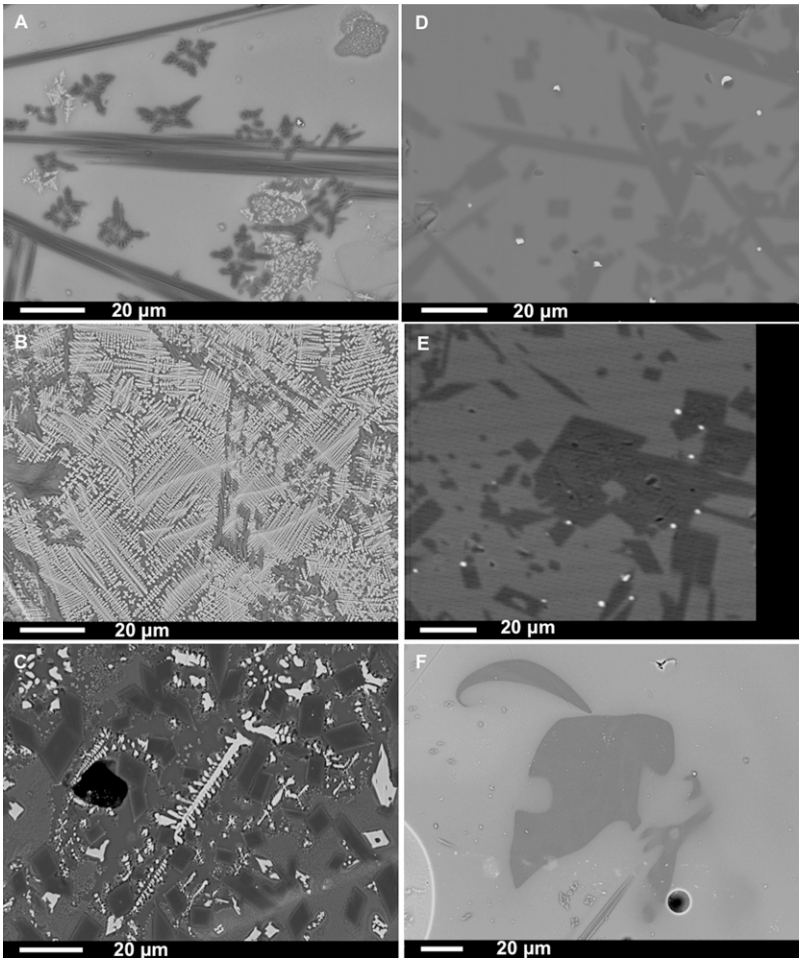

Fig. 2. Polished section SEM-BSE images of crystalline textures in magnetic spherules from the inferred YDB layer in Melrose, PA. (*A*) Lath-like mullite crystals and skeletal crystallites with swallowtails. (*B*) Bright herringbone-shaped Fe cordierite in glass in object 1. (*C*) Bright herringbone texture of hercynite–magnetite and dark mullite crystals, showing reaction rims in object 12. (*D*) Mullite crystals and Fe droplets. (*E*) Corundum crystals and Fe droplets in object 7. (*F*) Flow texture of quartz in object 6.

combined with the bulk chemical and REE composition indicate that the spherules formed from ancient upper continental crustal rocks.

Analyses of unleached and leached spherules show them to be enriched in Os with $^{187}Os/^{188}Os$ ratios that are much lower than the upper crustal Os isotope ratio of 1.3 (Table 1). Significantly, the dilute HCl leachate contains ~30% of the total amount of Os for each sample. A comparison of the leachate–residue pairs shows that the estimated leachate Os concentrations are 150–598 times higher than those of the corresponding residues. The $^{187}Os/^{188}Os$ ratios of the leachates range from 0.112 to 0.120. In comparison, a majority of meteorites have $^{187}Os/^{188}Os$ ratios ≥0.124 (32). Indeed, only a few meteorite samples have $^{187}Os/^{188}Os$ ratios between 0.120 and 0.124, and only two display $^{187}Os/^{188}Os$ ratios of 0.117 (36, 37). Koeberl et al. (38) reported a low $^{187}Os/^{188}Os$ ratio of 0.113 for a melt rock from the 66-Ma Chixculub impact crater. However, this low ratio has not been found in any of the other samples from Chixculub and is difficult to explain (39).

Discussion

The Os isotope ratios for a number of YDB bulk sediments and magnetic grains do not provide evidence of a meteoritic signal. In addition, data from Blackwater Draw bulk sediment and Gainey magnetic grain indicate that a five- to sixfold enrichment in Os concentration above the usually quoted background value of ~31 pg/g by itself is not evidence for a meteorite input. The observed $^{187}Os/^{188}Os$ ratio of YDB-age (20) bulk sediment at Melrose (= 0.42) is intriguing as the sediment also contains large spherules with high-temperature phases (see below and also refs. 20, 33). In the following sections, we examine the mineralogical and geochemical evidence and discuss the origin and provenance of the Melrose spherules.

Formation Conditions of Melrose Spherules. All objects from Melrose display features that are consistent with melting and quenching while in flight (Fig. 1): Three objects show welding of two even-sized (no. 1) or uneven-sized spherules (nos. 6 and 10); another object (no. 12) is tear-shaped. A common feature of all objects is a high abundance of rounded vesicles (Fig. 1), which may represent air bubbles or out-gassing of volatiles trapped in the silicate melt during quenching. Because the bulk glass composition of all spherules is dominated by SiO_2, Al_2O_3, and FeO (Table S3), the phase relations in the SiO_2-Al_2O_3-FeO system (40) can be used to assess the minimum temperature when the glass was molten. The upper bound of temperature of formation of some of these objects can be obtained from surviving high-temperature phases (iron droplets, lechatelierite, suessite, and corundum). In addition, the glass composition could be used to estimate the viscosity of the molten precursors at a given temperature and the glass transition temperature, using the formalism proposed by ref. 41.

The crystallization temperature of oxidized spherules (objects 1 and 12) is estimated to be ~1,550 °C (Fig. S5). The estimated viscosity (η in Pa/s) of molten precursors of these objects is quite low (at 1,200 °C $\log \eta = 1$ and 2.7 for objects 12 and 1, respectively). Their glass transition temperature is ~730 °C. In comparison, the lower limit of crystallization temperature of reduced spherules (objects 6, 7, and 10) ranges from ~1,600 °C to 1,700 °C (Fig. S5). Object 6 shows silica flow texture (lechatelierite, temperature >1,713 °C), object 7 contains droplets of iron (temperature >1,536 °C) and corundum and mullite (cocrystallization

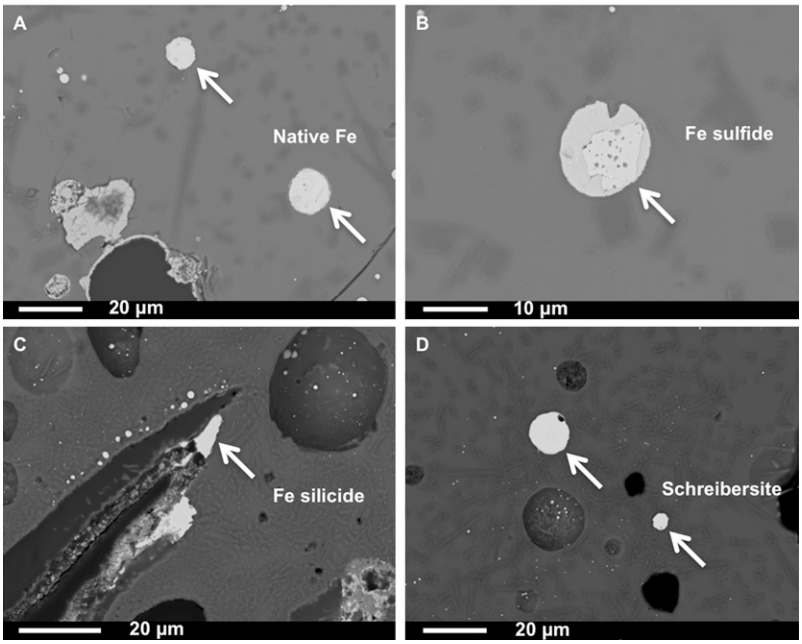

Fig. 3. Polished section BSE images containing different Fe forms in reduced magnetic spherules (objects 7 and 10) from the inferred YDB layer at Melrose. (*A*) Native Fe in object 7. (*B*) Exsolution in Fe sulfide into two phases (nonstoichiometric) in object 7. (*C*) Suessite (Fe-Ni silicide) in object 10. (*D*) Nonstoichiometric schreibersite (Fe-Ni phosphide) in object 10.

temperature of ~1,800 °C for the inferred bulk composition of this spherule), and object 10 has suessite that requires a crystallization temperature in excess of 2,000 °C (20, 42). The estimated viscosity of molten precursors of these objects is also quite high (at 1,200 °C $\log \eta = 5.1$, 4.2, and 4.8 for objects 6, 7, and 10, respectively) and their glass transition temperature is ~800 °C. The formation of nonstoichiometric schreibersite, suessite, and iron droplets requires extremely high temperatures and also rather low fO_2 prevalent during their formation. The high inferred temperatures, the low fO_2, and the presence of crystallites and glass are consistent with the spherules resulting from expansion, rapid cooling, and condensation within an impact fireball (43) (see below).

Origin of Melrose Spherules. The high temperature of formation of the spherules and absence of volcanism on the east coast of the United States indicate that the spherules are not diagenetic or volcanic in origin. The bulk chemical and REE composition of the spherules and their Sr and Nd isotopes unambiguously indicate that they did not originate from a meteorite and are terrestrial. Another possibility is that the magnetic spherules were formed in forest fires. However, the presence of suessite indicates that the formation temperatures should be in excess of 2,000 °C, which cannot be achieved by forest fires. We also considered whether the spherules could be produced from coal combustion, which has been ubiquitous in the environment since the Industrial Revolution. The bulk composition of coal is similar to that of the analyzed spherules (Fig. S5). Coal contains clay minerals (kaolinite and illite), quartz, and pyrite as impurities that break down when coal is heated/burned, leading to the formation of several new high-temperature minerals (40, 44, 45). During the spontaneous burning of coal spoil heaps/coal seams and coke making, the temperatures could go up to 1,200 °C. Under these conditions mullite, cordierite, and spinel form along with a number of other rare minerals (45, 46). The temperature during coal burning in power plants could reach 1,500 °C and fly ash containing glass spherules with magnetite has been reported (47). The coke charged in blast furnaces along with iron ore and flux takes part in complex solid-to-solid, solid-to-melt, and solid-to-gas reactions (48). The temperature at the tuyere level where hot air is blown into the blast furnace exceeds 2,000 °C and samples of tuyere coke taken from operating blast furnaces show a number of high-temperature minerals, including iron silicides, iron phosphides, sulphide, corundum, and even pure spinel (48). So blast furnaces could produce silicate glass spherules bearing iron silicides and phosphides. However, there has never been a blast furnace within <50 km of rural Melrose. In addition, the Melrose objects were found buried just above fragipan that marked the top of the late-Wisconsian permafrost table (20) (Fig. S1). Thus, the field evidence also precludes an anthropogenic origin for the spherules. In summary, the gross texture, mineralogy, and geochemistry of the Melrose spherules are inconsistent with an origin by diagenesis, volcanism, anthropogenesis, and meteoritic ablation. Rather, the spherules appear to have been produced from silicate melts generated during an impact. Because the spherules are glassy with rotational forms, vesicles, and crystallites, they are likely impact ejecta and have features of both microtektites and microkrystites (49).

Tektites associated with several inferred impacts show REE patterns and Sr and Nd isotopes indicative of their terrestrial provenance (e.g., refs. 50–52). Some of these objects have also been examined for their PGEs and Os isotopes and found to have high concentrations of Ir and/or Os with low $^{187}Os/^{188}Os$

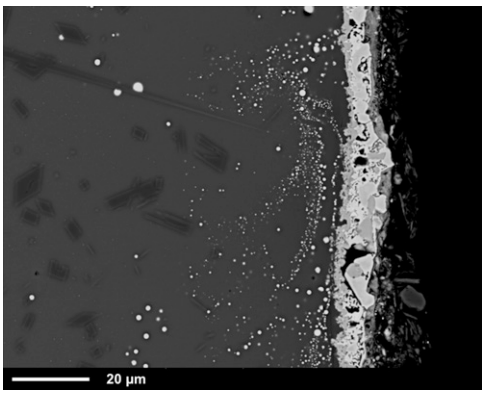

Fig. 4. SEM-BSE image showing the rim of object 7. The gray area is aluminosilicate material containing light-colored elemental Fe droplets. The spherule is coated with a light-colored, Fe-rich surface shell. Iron droplets are enriched near the rim and show flow orientation, possibly caused by spherule rotation while in a molten state.

ratios that are consistent with PGE contributions from a meteorite (49). For example, the Ivory Coast tektites contain 55–300 pg/g Os with $^{187}Os/^{188}Os$ ratios of 0.15–0.21, indicating a meteorite contribution of up to 0.6% (53). In comparison, two unleached Melrose spherules (objects 3 and 8, Table 1) have [Os] of 109 and 309 pg/g with $^{187}Os/^{188}Os$ ratios of 0.34 and 0.64, respectively. Leached Melrose spherules (objects 2, 4, 5, 11, and 13, Table 1) have [Os] of 55–126 pg/g with $^{187}Os/^{188}Os$ ratios of 0.14–0.75. At face value, these data suggest derivation from a meteorite. However, there is an alternate interpretation for the low Os isotope ratios. Our leaching experiments with spherules reveal that a large inventory of rather unradigenic Os in the spherules resides at or near the surface, where it is associated with reduced iron (Table 1 and Fig. 4). The following scenarios can be envisioned to account for the surface Os enrichment that accompanied spherule formation from target rocks following the impact: (*i*) accretion of impactor material with high concentration of Os onto the spherules inside the fireball; (*ii*) accretion of target material with high concentration of Os onto the spherules inside the fireball; and (*iii*) selective migration of terrestrial Os from the molten cores to the outer rims or, more broadly, selective extraction of terrestrial Os from silicate melts and its accretion onto spherules.

The surface $^{187}Os/^{188}Os$ ratios of the spherules are rather unradiogenic, suggesting that Os is likely not meteorite derived. If Os in the Melrose spherule leachates were of terrestrial origin, it would have to be sourced from an ancient terrain with extremely low time-integrated Re/Os ratio. A lower bound on the terrestrial mantle separation age of the Os source (54) of the leachates can be calculated by assuming that the Re/Os ratio of this source was zero after it separated from the mantle. The mantle separation age for the most radiogenic leachate (object 4) is ≥1.1 Ga. It is ≥2.4 Ga for the least radiogenic leachate (object 13). Surprisingly, these bounds incorporate those derived from Sm-Nd isotope systematics of the residues (1.4–1.8 Ga, Table 2), further suggesting a terrestrial origin of Os. As discussed below, the impact crater for the Melrose and Newtonville spherules probably lies within the Quebecia terrain within the Grenville Province. This terrain does not, however, contain ancient ultramafic/ophiolite complexes or PGE-rich ore bodies, which could be a source of large amounts of unradiogenic Os (Fig. S6). These considerations eliminate scenarios *i* and *ii* and suggest Os mobilization within the fireball may have led to its enrichment at the spherule surface.

Experiments (55) and theoretical considerations (43) indicate that impact-induced vaporization of target material results in a rapidly expanding fireball with low fO_2 forming reduced iron melts, which concentrate on or near the surface of melted tektites due to metal/silicate immiscibility or are completely lost.** Because Os is siderophile, it will partition into Fe melt and get enriched at the surface as well. Osmium enrichment accompanying iron melts has been observed in stony micrometeorites that have been flash-heated while traveling through the earth's atmosphere. These objects display variable loss of Fe and Os via selective migration of reduced iron melts to the surface of the spherules that also remove Os from the interior of the spherules.††

Provenance of Melrose Spherules. A 4-km diameter impact crater with an estimated age 12.9 ka† was found off Corossol Island near the city of Sept Iles, Gulf of St. Lawrence, Canada. The Corossol Crater is the largest known crater within the last 900,000 y, is the largest in North America in the last 35 My, and is ∼1,200 km away from the Melrose site. The impact occurred in Ordovician limestones that overlie the 564-Ma Sept Iles intrusive suite†. The impact may have also excavated the rocks from the intrusive suite. We explored the Corossol Crater as the source of the Melrose spherules. From the Sr isotope evolution of seawater it is evident that the $^{87}Sr/^{86}Sr$ ratio of Ordovician carbonates should range from 0.708 to 0.709 (56). These values are much lower than those observed in Melrose spherules. Similarly, the whole-rock Sr isotope ratios from the Sept Iles Intrusion (= 0.7038 on average) are much lower than those of the Melrose spherules. The lithologies underlying the Corossol Crater are therefore not the source of Melrose spherules.

The depleted mantle Nd model ages for the Melrose spherules (T_{DM}) range from 1.4 Ga to 1.8 Ga (Table 2). These ages suggest that the target is Grenvillean in age. Intriguingly, the measured ε_{Nd} values of the spherules (and also of the microspherule cluster from Newtonville) are identical to those measured for the Grenville age gray gneisses exposed just north and west of the Corossol Crater (57, 58). Using the Nd isotope model age map of Grenville from Dickin (57), we find that the spherule model ages are consistent with the target being in the "Quebecia" (Fig. S6), which is a Mesoproterozoic arc terrain consisting mainly of massif anorthosites, gabbros, and granitic gneisses. Because the Corossol Crater also lies within the Quebecia terrain, we suggest that there were more than one impact in this region that were closely associated in time. The spherules are not enriched in Ca and lack a pronounced positive Eu anomaly that is found associated with Grenvillean anorthosites and so we can preclude this lithology being the target. As the spherules display chondrite-normalized light REE-enriched patterns with negative Eu anomalies and unradiogenic $^{187}Os/^{188}Os$ ratios the target rocks could be a mixture of weathered gabbros and granitic gneisses with Re/Os ∼ 0.

An alternative scenario to the above could also be suggested. The Laurentide Ice Sheet flowed from the north in Quebec through the Laurentide channel past Anticosti Island and into the Atlantic Ocean (59, 60). Just before the Younger Dryas, the ice sheet had retreated rapidly close to the north shore of the present St. Lawrence estuary (Fig. S6). However, the extent to which the ice sheet occupied the future Corossol impact crater site is not clear at this time due to a lack of detailed paleogeographic reconstruction. Regardless, it is likely that till from the Quebecia terrain occupied the area during the impact. The extent to which pre-YDB sediment was present in the St. Lawrence estuary around Sept Iles is not known. A recent study combines seismic reflection data, multibeam bathymetry, and core and chronostratigraphic data to infer that ∼26–93 m of pre-Holocene till was deposited in the Lower St. Lawrence estuary farther to the west of Sept Iles (61). If Quebecia-derived till blanketed the Ordovician limestone around Sept Iles at the time of the Corossol impact, it could be the source of Melrose (and Newtonville) spherules. However, this scenario is less likely as the expected $^{187}Os/^{188}Os$ ratio of the Quebecia till is ∼1.3. The Quebecia terrain is therefore the likely source of Melrose (and Newtonville) spherules. A search should be conducted to locate other craters in this region.

Spherules from Other Localities and the Nature of Impact at the YDB. Impact spherules are millimeter-scale glassy bodies that form from melt and vapor condensate droplets deposited at a distance greater than ∼10 crater diameters (49). Impact-related melt glass and spherules appear to be widely distributed at YDB sites including Melrose, providing evidence for multiple ET impacts 12.9 ka (20, 23, 26). As seen in this study, the spherules from Melrose display evidence of high-temperature melting of sediment derived from ancient upper continental crust and rapid quenching. The Os isotopes of the spherules, although unradiogenic, also indicate derivation from ancient continental crust.

Because we do not find evidence of ET Os input in any of the sediment archives, the key question then is, What is the nature of the YDB impactor? It has been suggested by Firestone et al. (10)

**Yakovlev OI, Dikov YP, Gerasimov MV, Wlotzka F, Huth J, The behavior of Pt in silicate melts during impact-simulated high temperature heating. 33rd Lunar and Planetary Science Conference, March 11–15, 2002, abstr 1271.

††Chen C, Taylor S, Sharma M, Iron and osmium isotopes from stony micrometeorites and implications for the Os budget of the ocean. 36th Lunar and Planetary Science Conference, March 14–18, 2005, abstr 2134.

that the YD impactor was a fragmented comet with additional supporting evidence coming from other reports (19, 20, 23, 26). Observations of extant comets suggest that they are loosely held-together aggregates with densities that are consistent with them not being made of pure ice (62). Indeed, the nuclei of comets are a mixture of ice, interstellar medium-derived amorphous silicates, and hot inner solar nebula-derived crystalline silicates (see review in ref. 63). Although it is likely that the Os concentration of comets is much lower than that of meteorites, it should still be high enough that the ET signal is registered at distances >10 times crater diameter. As an example, if the 4-km Corossol Crater in Sept Iles was created by a 45° impact of a comet with a density of 1 g/cm^3 and traveling at speed of 40 km/s, the diameter of the impactor would be ∼300 m (http://impact.ese.ic.ac.uk/ImpactEffects) (64). If this comet were a mixture of 75% ice and 25% chondritic silicate particles, its expected Os concentration would be about 124 ng/g. If Os from this impactor were to be mixed in a 1-cm-thick layer over a circular region 270 km in radius (68 times crater diameter), then there will be a 100-fold dilution by continental material, erasing any evidence of ET Os.

Absence of an unequivocal ET signal from our Os isotope data and those of Paquay et al. (28) is thus intriguing as it indicates that Os delivered by impactors at the YDB was overwhelmed by the terrestrial Os. The archives that receive little terrestrial input such as the Greenland ice cores could therefore be used in estimating the extent of global PGE deposition at the YDB. Such data have been confounded by imprecise timing of the onset of Younger Dryas in ice cores from the Greenland Ice Sheet Project (GISP-2) and Greenland Ice Core Project (GRIP) (refs. 65 and 66 and references therein) that were drilled in proximity to each other at Summit, Greenland. A low-resolution record of Ir and Pt deposition from the GRIP ice core shows Ir concentration of 0.25 fg/g with a chondritic Pt/Ir ratio of 2.4 at 12.843 ka (67). In comparison, a recent high-resolution record investigating PGE deposition from across Bølling–Allerød to Younger Dryas using the GISP-2 ice core finds an Ir concentration of 80 fg/g with a superchondritic Pt/Ir ratio of 1,000 at the onset of Younger Dryas at 12.882 ka.[‡‡] At face value these two data appear to be incommensurate to each other. However, an offset of 180 y has been inferred between the δ^{18}O-based time horizons that mark the onset of Younger Dryas in the GISP-2 (= 12.882 ka) and GRIP (= 12.702 ka) ice cores (65). We find that in terms of GISP-2 chronology, the low-resolution GRIP sample corresponds to 13.023 ka and is therefore much older. The GISP-2 data suggest the impact of a subkilometer-size iron meteorite that increased the Pt and Ir fluences but with a Pt/Ir ratio of 1,000. The results of our study indicate enrichment of terrestrial Os accompanying selective volatilization and separation of iron melts from silicate melts in the impact fireball. Extending this observation to other PGEs, we suggest that highly fractionated Pt/Ir ratios observed in Greenland ice could also be terrestrial. Further assessments of the PGE fluence at YDB by combining Pt and Ir measurements with Os concentration and isotope composition in Greenland ice cores should provide much more robust insights into the nature of the YDB impactor(s).

Conclusions

Our geochemical analyses of materials from the YDB layer have led to the following main conclusions:

i) Bulk sediment samples from most YDB study sites in North America and Europe do not reveal an expected ET anomaly in Os concentrations. Significantly, the Os isotope ratios in the sediments from most of the sites are highly radiogenic, ranging from 1.4 to 3.0, and are consistent with a terrestrial origin. The two exceptions from Lommel, Belgium and Melrose, PA give ^{187}Os/^{188}Os ratios much lower than that of the average upper continental crust.

ii) Although we can rule out volcanic contribution for YDB at Lommel as a source of low ^{187}Os/^{188}Os ratio, we cannot unequivocally demonstrate the absence of any ET Os as we have not found magnetic grains with a high concentration of Os. When it is combined with Os isotopes in the magnetic grain separates, we conclude that the low ^{187}Os/^{188}Os ratio is likely due to the derivation from source with time-integrated Re/Os ratio lower than that of average continental crust.

iii) The YDB site at Melrose yielded small magnetic spherules as well as large spherules. The latter are enriched in Os and have ^{187}Os/^{188}Os ratios that are, in general, much lower than those of the bulk sediment. Detailed petrochemical analyses of the objects indicate temperature of formation >2,000 °C, consistent with an extraterrestrial impact as also inferred by ref. 20. Bulk major element chemical composition of the spherules is dominated by SiO_2, Al_2O_3, and FeO. Their REE patterns are similar to those of average upper continental crust. The Sr isotope analyses of the spherules appear to preclude the possibility of the recently reported Corossol Crater in Sept Iles as being the impact target. Instead, our data indicate that the Melrose spherules come from another target in close proximity to the Corossol Crater, which lies within the 1.5-Ga Quebecia terrain. Our evidence thus suggests that the impact took place near the southern margin of the Laurentide Ice Sheet (Fig. S6).

iv) Our findings are consistent with the hypothesis of Firestone et al. (10) that multiple impacts occurred at ∼12.9 ka (YD onset), centered in the northeastern United States. It is intriguing that these impacts were part of a number of other impacts around the globe that produced spherules with high-temperature minerals (20, 23, 26) but with little enrichment in PGEs.

Materials and Methods

Details of sampling sites, magnetic fraction separation, SEM and Electron Probe Micro-Analyzer (EPMA) work, clean laboratory protocols, and mass spectrometry are given in *SI Text*. Briefly, we selected samples from Blackwater Draw, Sheriden Cave, Murray Springs, Gainey, and Lommel as these sites were well documented by Firestone et al. (10). In addition to these sites, we also selected samples from Melrose and Newtonville as they both yielded magnetic spherules from horizons that are late Wisconsian. These two sites have limited age control at this time. Thin sections of objects from these sites were examined using an SEM at Dartmouth College. Selected large objects were then subsequently analyzed using an electron probe at the University of Massachusetts, Amherst. Bulk sediment samples were crushed and homogenized in a zirconia mill. They were dissolved in reverse-aqua regia, using a High-Pressure Asher. Osmium was extracted using liquid Br_2 and then purified using microdistillation. Individual magnetic grains/spherules or grain clusters were dissolved using the above procedure, which was modified to separate Sr, Sm, and Nd. Osmium, Sr, Sm, and Nd isotopes were measured using standard procedures that are given in *SI Text*.

ACKNOWLEDGMENTS. We thank A. West for providing us with the bulk samples and the magnetic separates from several YDB sites. The Melrose spherules and other melt materials were discovered by Yvonne Malinowski in her backyard in northeastern Pennsylvania. She was a gracious hostess for our numerous trips to her home and property. We also thank Douglas Kennett for providing a sample of Laacher See volcanics. We thank Charles Daghlian (Ripple Electron Microscope Facility, Dartmouth Medical School) for training Y.W. at the SEM. Quantitative analyses of minerals and their identification were done at the Electron Microscope facility at the Department of Geology, University of Massachusetts, Amherst. This work could not have been accomplished without the help and generosity of Mike Jercinovic. We also thank Michael Higgins for sending us unpublished Sr isotope data for the Sept Iles intrusion. An earlier version of this paper was informally reviewed by Jim Kennett and Jason Moore whose comments and suggestions led to a substantially improved manuscript. We also thank three anonymous reviewers for their perceptive comments. Funding for this study was provided by National Science Foundation–Earth Sciences (EAR) 0948426.

[‡‡]Petaev MI, Huang S, Jacobsen SB, Zindler A. Large platinum anomaly in the GISP2 ice core: Evidence for a cataclysm at the Bølling-Allerød/Younger Dryas boundary? 44th Lunar and Planetary Science Conference, March 18–22, 2013, abstr 1719.

1. Haynes CV, Jr. (2008) Younger Dryas "black mats" and the Rancholabrean termination in North America. *Proc Natl Acad Sci USA* 105(18):6520–6525.
2. Kennett DJ, et al. (2008) Wildfire and abrupt ecosystem disruption on California's Northern Channel Islands at the Ållerød-Younger Dryas boundary (13.0-12.9 ka). *Quat Sci Rev* 27(27–28):2530–2545.
3. Kennett JP, West A (2008) Biostratigraphic evidence supports Paleoindian population disruption at approximately 12.9 ka. *Proc Natl Acad Sci USA* 105(50):E110–E110, author reply E112–E114.
4. Broecker WS, Denton GH (1989) The role of ocean-atmosphere reorganizations in glacial cycles. *Geochim Cosmochim Acta* 53(10):2465–2501.
5. Broecker WS, et al. (1989) Routing of meltwater from the Laurentide ice-sheet during the Younger Dryas cold episode. *Nature* 341(6240):318–321.
6. Kennett JP, Shackleton NJ (1975) Laurentide ice sheet meltwater recorded in gulf of Mexico deep-sea cores. *Science* 188(4184):147–150.
7. Murton JB, Bateman MD, Dallimore SR, Teller JT, Yang Z (2010) Identification of Younger Dryas outburst flood path from Lake Agassiz to the Arctic Ocean. *Nature* 464 (7289):740–743.
8. Broecker WS, Rooth C, Peng TH (1985) Ventilation of the deep northeastern Atlantic. *J Geophys Res Oceans* 90(NC4):6940–6944.
9. Condron A, Winsor P (2012) Meltwater routing and the Younger Dryas. *Proc Natl Acad Sci USA* 109(49):19928–19933.
10. Firestone RB, et al. (2007) Evidence for an extraterrestrial impact 12,900 years ago that contributed to the megafaunal extinctions and the Younger Dryas cooling. *Proc Natl Acad Sci USA* 104(41):16016–16021.
11. Kennett DJ, et al. (2009) Nanodiamonds in the Younger Dryas boundary sediment layer. *Science* 323(5910):94.
12. Daulton TL, Pinter N, Scott AC (2010) No evidence of nanodiamonds in Younger-Dryas sediments to support an impact event. *Proc Natl Acad Sci USA* 107(37):16043–16047.
13. Scott AC, et al. (2010) Fungus, not comet or catastrophe, accounts for carbonaceous spherules in the Younger Dryas "impact layer". *Geophys Res Lett* 37(14):L14302.
14. Pinter N, et al. (2011) The Younger Dryas impact hypothesis: A requiem. *Earth Sci Rev* 106(3–4):247–264.
15. Daulton TL (2012) Suspect cubic diamond "impact" proxy and a suspect lonsdaleite identification. *Proc Natl Acad Sci USA* 109(34):E2242–E2242, author reply E2245–E2247.
16. Stoffler D, Langenhorst F (1994) Shock metamophism of quartz in nature and experiment. 1. Basic observation and theory. *Meteoritics* 29(2):155–181.
17. Koeberl C (2007) The geochemistry and cosmochemistry of impacts. *Treatise of Geochemistry*, ed Davis A (Elsevier, New York). Online edition, Vol 1.28, pp 1–52.
18. French BM, Koeberl C (2010) The convincing identification of terrestrial meteorite impact structures: What works, what doesn't, and why. *Earth Sci Rev* 98(1–2):123–170.
19. Israde-Alcántara I, et al. (2012) Evidence from central Mexico supporting the Younger Dryas extraterrestrial impact hypothesis. *Proc Natl Acad Sci USA* 109(13):E738–E747.
20. Bunch TE, et al. (2012) Very high-temperature impact melt products as evidence for cosmic airbursts and impacts 12,900 years ago. *Proc Natl Acad Sci USA* 109(28): E1903–E1912.
21. Holcombe TL, Warren JS, Reid DF, Virden WT, Divins DL (2001) Small rimmed depression in Lake Ontario: An impact crater? *J Great Lakes Res* 27(4):510–517.
22. Spooner I, et al. (2009) Identification of the Bloody Creek structure, a possible impact crater in southwestern Nova Scotia, Canada. *Meteorit Planet Sci* 44(8):1193–1202.
23. Wittke JH, et al. (2013) Evidence for deposition of 10 million tonnes of impact spherules across four continents 12,800 y ago. *Proc Natl Acad Sci USA* 110(23): E2088–E2097.
24. Mahaney WC, et al. (2008) Evidence for a Younger Dryas glacial advance in the Andes of northwestern Venezuela. *Geomorphology* 96(1–2):199–211.
25. Fayek M, Anovitz LM, Allard LF, Hull S (2012) Framboidal iron oxide: Chondrite-like material from the black mat, Murray Springs, Arizona. *Earth Planet Sci Lett* 319: 251–258.
26. LeCompte MA, et al. (2012) Independent evaluation of conflicting microspherule results from different investigations of the Younger Dryas impact hypothesis. *Proc Natl Acad Sci USA* 109(44):E2960–E2969.
27. Surovell TA, et al. (2009) An independent evaluation of the Younger Dryas extraterrestrial impact hypothesis. *Proc Natl Acad Sci USA* 106(43):18155–18158.
28. Paquay FS, et al. (2009) Absence of geochemical evidence for an impact event at the Bølling-Allerød/Younger Dryas transition. *Proc Natl Acad Sci USA* 106(51):21505–21510.
29. Haynes CV, Jr., et al. (2010) The Murray Springs Clovis site, Pleistocene extinction, and the question of extraterrestrial impact. *Proc Natl Acad Sci USA* 107(9):4010–4015.
30. Alvarez LW, Alvarez W, Asaro F, Michel HV (1980) Extraterrestrial cause for the cretaceous-tertiary extinction. *Science* 208(4448):1095–1108.
31. Turekian KK (1982) Potential of $^{187}Os/^{186}Os$ as a cosmic versus terrestrial indicator in high indium layers of sedimentary strata. *Geol Soc Amer Spec Pap* 190:243–250.
32. Sharma M (2011) Applications of osmium and iridium as biogeochemical tracers in the environment. *Handbook of Environmental Isotope Geochemistry*, Advances in Isotope Geochemistry, ed Baskaran M (Springer, Berlin), pp 205–227.
33. Wu Y (2011) Origin and provenance of magnetic spherules at the Younger Dryas boundary. MS thesis (Dartmouth College, Hanover, NH).
34. Gromet LP, Dymek RF, Haskin LA, Korotev RL (1984) The North-American Shale Composite-its compilation, major and trace-element characteristics. *Geochim Cosmochim Acta* 48(12):2469–2482.
35. Condie KC (1993) Chemical composition and evolution of the upper continental crust: Contrasting results from surface samples and shales. *Chem Geol* 104(1-4):1–37.
36. Rankenburg K, Brandon AD, Humayun M (2007) Osmium isotope systematics of ureilites. *Geochim Cosmochim Acta* 71(9):2402–2413.
37. van Acken D, Brandon AD, Lapen TJ (2012) Highly siderophile element and osmium isotope evidence for postcore formation magmatic and impact processes on the aubrite parent body. *Meteorit Planet Sci* 47(10):1606–1623.
38. Koeberl C, et al. (1994) Evidence for a meteoritic component in impact melt rock from the Chicxulub structure. *Geochim Cosmochim Acta* 58(6):1679–1684.
39. Gelinas A, et al. (2004) Osmium isotope constraints on the proportion of bolide component in Chicxulub impact melt rocks. *Meteorit Planet Sci* 39(6):1003–1008.
40. Huggins FE, Kosmack DA, Huffman GP (1981) Correlation between ash-fusion temperatures and ternary phase-diagrams. *Fuel* 60(7):577–584.
41. Giordano D, Russell JK, Dingwell DB (2008) Viscosity of magmatic liquids: A model. *Earth Planet Sci Lett* 271(1–4):123–134.
42. Rietmeijer FJM, et al. (2008) Origin and formation of iron silicide phases in the aerogel of the Stardust mission. *Meteorit Planet Sci* 43(1–2):121–134.
43. Lukanin OA, Kadik AA (2007) Decompression mechanism of ferric iron reduction in tektite melts during their formation in the impact process. *Geochem Int* 45(9): 857–881.
44. Huffman GP, Huggins FE (1986) Reactions and transformations of coal mineral matter at elevated temperatures. *ACS Symp Ser* 301:100–113.
45. Gornostayev S, Kerkkonen O, Harkki J (2009) Behaviour of coal associated minerals during coking and blast furnace processes - a review. *Steel Res Int* 80(6):390–395.
46. Sokol E, Volkova N, Lepezin G (1998) Mineralogy of pyrometamorphic rocks associated with naturally burned coal-bearing spoil-heaps of the Chelyabinsk coal basin, Russia. *Eur J Mineral* 10(5):1003–1014.
47. Ramsden AR, Shibaoka M (1982) Characterization and analysis of individual fly-ash particles from coal-fired power-stations by a combination of optical microscopy, electron-microscopy, and quantitative electron micro-probe analysis. *Atmos Environ* 16(9):2191–2206.
48. Gornostayev S, Harkki J (2005) Spinel crystals in tuyere coke. *Metall Mater Trans B Process Metall Mater Proc Sci* 36(2):303–305.
49. Glass BP, Simonson BM (2012) Distal impact ejecta layers: Spherules and more. *Elements* 8(1):43–48.
50. Shaw HF, Wasserburg GJ (1982) Age and provenance of the target materials for tektites and possible impectites as inferred from Sm-Nd and Rb-Sr systematics. *Earth Planet Sci Lett* 60(2):155–177.
51. Blum JD, Papanastassiou DA, Koeberl C, Wasserburg GJ (1992) Neodymium and strontium isotopic study of Australasian tektites—New constrains on the provenance and age of target materials. *Geochim Cosmochim Acta* 56(1):483–492.
52. Koeberl C (1994) Tektite origin by hypervelocity asteroidal and cometary impact: Target rocks, source craters, and mechanisms. *Large Meteorite Impacts and Planetary Evolution*, eds Dressler BO, Grieve RAF, Sharpton VL (Geological Society of America, Boulder, CO), Special Paper 293, pp 133–151.
53. Koeberl C, Shirey SB (1993) Detection of a meteoritic component in ivory coast tektites with rhenium-osmium isotopes. *Science* 261(5121):595–598.
54. Shirey SB, Walker RJ (1998) The Re-Os isotope system in cosmochemistry and high-temperature geochemistry. *Annu Rev Earth Planet Sci* 26:423–500.
55. Gerasimov MV, Yakovlev OI, Dikov YP, Wlotzka F (2005) Evaporative differentiation of impact-produced melts: Laser-simulation experiments and comparison with impact glasses from the Logoisk crater. *Geol Soc Amer Spec Pap* 384:351–366.
56. Prokoph A, Shields GA, Veizer J (2008) Compilation and time-series analysis of a marine carbonate delta(18)O, delta(13)C, (87)Sr/(86)Sr and delta(34)S database through Earth history. *Earth Sci Rev* 87(3–4):113–133.
57. Dickin AP (2000) Crustal formation in the Grenville Province: Nd-isotope evidence. *Can J Earth Sci* 37(2):165–181.
58. Dickin AP, Higgins MD (1992) Sm/Nd evidence for a major 1.5 Ga crust-forming event in the Central Grenville Province. *Geology* 20(2):137–140.
59. Shaw J, et al. (2006) A conceptual model of the deglaciation of Atlantic Canada. *Quat Sci Rev* 25(17–18):2059–2081.
60. Josenhans H, Lehman S (1999) Late glacial stratigraphy and history of the Gulf of St. Lawrence, Canada. *Can J Earth Sci* 36(8):1327–1345.
61. Duchesne MJ, et al. (2010) Role of the bedrock topography in the Quaternary filling of a giant estuarine basin: The Lower St. Lawrence Estuary, Eastern Canada. *Basin Res* 22(6):933–951.
62. Weissman PR, Lowry SC (2008) Structure and density of cometary nuclei. *Meteorit Planet Sci* 43(6):1033–1047.
63. Mumma MJ, Charnley SB (2011) The chemical composition of comets-Emerging taxonomies and natal heritage. *Annual Review of Astronomy and Astrophysics*, eds Faber SM, VanDishoeck E (Annual Reviews, Palo Alto, CA), Vol 49, pp 471–524.
64. Collins GS, Melosh HJ, Marcus RA (2005) Earth Impact Effects Program: A Web-based computer program for calculating the regional environmental consequences of a meteoroid impact on Earth. *Meteorit Planet Sci* 40(6):817–840.
65. Southon J (2004) A radiocarbon perspective on Greenland ice-core chronologies: Can we use ice cores for (14)C calibration? *Radiocarbon* 46(3):1239–1259.
66. Southon J (2002) A first step to reconciling the GRIP and GISP2 ice-core chronologies, 0-14,500 yr BP. *Quat Res* 57(1):32–37.
67. Gabrielli P, et al. (2004) Meteoric smoke fallout over the Holocene epoch revealed by iridium and platinum in Greenland ice. *Nature* 432(7020):1011–1014.

Supporting Information

Wu et al. 10.1073/pnas.1304059110

SI Text

Blackwater Draw (NM), Sheriden Cave (OH), Murray Springs (AZ), Gainey (MI), and Lommel (Belgium)

These five Clovis-age sites were the same sites described in Firestone et al. (1). They were selected because they are well dated and documented by previous studies (1). Two of them are type sites: the Clovis-point style at Blackwater Draw, NM and the Gainey-point style at Gainey, MI (1). Each site is underlain by a Younger Dryas boundary (YDB) layer (average thickness of 3 cm) (1). At Blackwater Draw and Murray Springs, AZ, the YDB is found beneath the black mat and overlies Clovis extinct megafaunal remains (1).

Melrose, PA

This sampling site, initially investigated by ref. 2 and also examined by Bunch et al. (3), is located in northeastern Pennsylvania, near the village of Melrose (41° 92′ 38.4″ N; 75° 50′ 31.4″ W) (Fig. S1*A*). Bulk sediment samples were collected from 0 to ∼40 cm, and the bottommost sample included channery loam fragipan. Channery silt loam colluvium from 28 to 40 cm included low levels of ∼70 magnetic spherules per kilogram. Atop the till, a carbon-rich 5-cm stratum from 23 to 28 cm was sampled, which is interpreted as including postglacial sediment that could include sediments from the Younger Dryas (YD) cooling interval, dated by Bunch et al. (3), but not well constrained. This layer contained ∼400 microspherules per kilogram. In comparison with the spherules from other YDB sites, these spherules are much larger (2–5 mm in diameter).

Newtonville, NJ

This site is a sand pit located in southern New Jersey (39° 34′ 4.6″ N; 74° 54′ 36.5″ W). The A-horizon is single-grain loamy sand that was recently bladed off and stockpiled. Two distinct loamy-sand horizons are present, separated by a clear wavy boundary (Fig. S1*B*). The first is an ashen-gray layer at 25–40 (50) cm below the present surface composed of organic matter, charcoal, and sand grains that are mostly coated with glass-like carbon. The second is a yellowish-brown layer at 40 (50) cm to 60 (120) cm that is low in organic matter, displaying no glasslike carbon coatings on grains. Its contact with underlying fragipan is abrupt and undulating due to cryoturbation during thermokarst ∼40–30 ka and marks the past permafrost table. Optically stimulated luminescence (OSL) dating of frost-crack infill (16.8 ± 1.7 ka) derived from the second horizon material indicates this cover-sand is late Wisconsian (4). A 10-cm-thick sample was taken from the bottom of the ashen-gray layer, and it contained 1,840 magnetic microspherules per kilogram, and a 10-cm-thick sample from the top of the yellow-brown layer contained 2,000 microspherules per kilogram. A third offset sample taken ∼100 cm deeper contained no detectable spherules.

Bulk Sample Collection and Magnetic Fraction Separation

Bulk samples from each site (Blackwater Draw, Murray Springs, Gainey, Sheriden Cave, and Lommel) were provided by A. West, a coworker in Firestone et al. (1). Each bulk sediment sample of 10 g was crushed by a zirconia ball mill and 1 g of sample was prepared for chemical separation. Magnetic fractions of each sample from the above sites were also provided by A. West. Magnetic grains were handpicked from the magnetic fractions at Dartmouth College, using a binocular microscope mounted on an *x-y* stage. Magnetic spherules from New Jersey and Pennsylvania were collected and individual objects were separated by Malcolm A. LeCompte.

Scanning Electron Microscopy and Electron Probe Analysis

Backscatter scanning electron microscopy (SEM) images of spherules from New Jersey and Pennsylvania were taken using the XL-30 field emission gun environmental scanning electron microprobe at the Electron Microscope Facility, Dartmouth College. Analyses were performed at 15 kV accelerating voltage with 4 μm of spot size. Six selected microspherule samples from Melrose were mounted on glass plates, ground down to expose an interior surface, polished, and carbon coated. Major oxide compositions were determined using a Cameca SX50 electron microprobe at the University of Massachusetts, Amherst. The acceleration voltage was 15 kV and the current was 20 nA. The spectra were corrected for background and normalized to 100 wt%, using the integrated software. The glass compositions of the samples were standardized to a glass standard. Most glass compositions are an average of five spot analyses.

Chemical Separation of Os, Sr, Nd, and Sm

High yield and low blank techniques developed in the Radiogenic Isotope Geochemistry Laboratory at Dartmouth College for Os isotope determination in water and Os isotope determination in cosmic dust were used to analyze the bulk sediments and magnetic spherules (5, 6). These techniques were combined with previously existing procedures. Fig. S3 gives a flow diagram of the complete protocol to purify Os, Sr, Nd, and Sm.

The bulk sediment samples were spiked with ^{190}Os spike to determine Os concentrations and Os isotopic ratios. Approximately 1 g of sediment sample, ^{190}Os spike, 3 mL of HCl, and 5 mL of HNO_3 were added into the carius tube and immediately sealed with a Teflon tape gasket and glass lid, which was secured with Teflon tape. The sealed carius tube was put in a High Pressure Asher (Anton Paar), pressurized to 100 bars, and heated to 300 °C for 16 h. Os was extracted using 2 mL (∼6.6 g) of liquid bromine and then reduced in 1.5 mL of HBr. The sample was gently dried and further purified by microdistillation.

Individual magnetic grains or spherules were cleaned in acetone, ethanol, and deionized water; air dried; and weighed on a microbalance. The individual objects were leached in 1 mL 1.5 N HCl with 5-min ultrasonication, rinsed with 2 mL Milli-Q water, air dried, weighed on the microbalance, and then gently crushed. The leached HCl and Milli-Q were combined together. The crushed spherules were spiked with ^{190}Os spike. The Os separation of the sample was the same as the bulk analyses but with different amounts of reagents (0.75 mL HCl, 1.25 mL HNO_3, 3 g bromine, and 0.75 mL HBr). The remainder solution from the bromine extraction was dried. Forty microliters of HF and 40 μL of HNO_3 were added and the solution was evaporated to dryness at 150 °C overnight. The sample was then redissolved in 2 mL of 1.5 N HCl. An aliquot (∼10%) was taken and Sr-Nd tracers were added to obtain approximate concentrations. After they were determined, the remaining 90% of solution was optimally spiked. The remaining 90% sample solution was then optimally spiked and processed through a cation exchange column to extract Sr and rare earth element (REE) fractions. The REE fraction was dried, redissolved in 40 μL of 0.75 N HCl, and loaded on a high-pressure (2.7 psi) cation exchange column packed with AG-50W X-4 resin. Nd and Sm fractions were eluted using α-hydroxyisobutyric acid (7).

Mass Spectrometry

Details of Os isotope measurements and concentration determinations are given in ref. 8. Briefly, the Os fraction of the sample in 1 μL of HBr was loaded on the precleaned Pt side filament, using a fine polypropylene tubing on a microsyringe, and dried at 0.8 A. The sample was loaded in the center of the filament typically in an area of about 1–2 mm^2. Three drops of fresh $Ba(OH)_2$ emitter solution were loaded on top of the sample and dried. The filament was then heated to 1.2 A for 6 s. Osmium isotopes were measured as OsO_3^- on a Triton thermal ionization mass spectrometer (TIMS), using the double-filament geometry developed by ref. 5. The data were corrected for oxygen isotope composition, mass fractionation, and [Os] estimated by isotope dilution.

Sr fraction was loaded on a W filament with HCl and H_2PO_4, using the Ta_2O_5 sandwich-loading technique. The load covered 4–5 mm of the filament length. The Sr isotopes were determined by TIMS analysis. The data were corrected off-line to determine the [Sr] by isotope dilution. Repeated measurements of Sr Standard Reference Material from the National Institute of Standards and Technology (NIST SRM 987) done during the course of these analyses gave an $^{87}Sr/^{86}Sr$ ratio of 0.710245 ± 0.000012 (2σ; $n = 13$).

Nd fraction was dried hard, using a hot plate and a heat lamp. Two methods were used to measure the Nd isotopes as NdO^+ on the Triton TIMS. In the first method, the sample was redissolved in 1 μL of concentrated HNO_3 and loaded on a Re center filament at 0.8 A. Then 1 μL Ta_2O_5-H_3PO_4 solution was loaded as an emitter to increase the intensity of NdO^+ ions (9). The filament was finally heated to glow red for 20 s. Ten loads of 1 ng Nd of a standard solution Caltech nNdβ standard yielded 0.1- to 0.3-V beams on $^{144}Nd^{16}O^+$ with $\varepsilon_{Nd} = -14.50 \pm 0.65$ (2σ, external reproducibility; $n = 10$). In the second method (7), the sample was redissolved in 1 μL of 2.5 N HCl and loaded on a Re center filament at 0.6 A. The filament was heated up slowly to 1.5 A and then to 2 A for 3 s. Five loads of 1 ng Nd of the Caltech nNdβ standard solution yielded 0.2- to 0.4-V beams on $^{144}Nd^{16}O^+$ with $\varepsilon_{Nd} = -14.32 \pm 0.60$ (2σ, external reproducibility; $n = 5$). The second method was used to load the Nd samples due to its higher intensity and stability of the signal. The data were corrected for oxygen isotope composition, mass fractionation, and [Nd] estimated by isotope dilution.

The Sm fraction was dried hard, using a hot plate and a heat lamp. The sample was loaded using the same method as the second Nd loading method. Samarium isotopes were analyzed on TIMS, using the Second Electron Multiplier. The typical intensity of $^{154}Sm^{16}O^+$ is ~10,000 counts per second at 1,200 °C. The $^{154}Sm^{16}O^+/^{147}Sm^{16}O^+$ ratio was used in the isotope dilution calculation of the Sm concentration.

Uncertainty Associated with Os Concentration Measured Using Isotope Dilution

The Os concentration is obtained from the measured ($^{188}Os/^{190}Os$) ratio, using isotope dilution that assumes complete equilibration between the sample and the tracer Os ("spike"):

$$\left[{}^{190}Os\right]_S = \left[{}^{190}Os\right]_T \cdot \left[\frac{\left(\frac{^{188}Os}{^{190}Os}\right)_T - \left(\frac{^{188}Os}{^{190}Os}\right)_M}{\left(\frac{^{188}Os}{^{190}Os}\right)_M - \left(\frac{^{188}Os}{^{190}Os}\right)_S}\right].$$

Here the subscripts S, T, and M refer to sample, tracer, and measured, respectively. The $[^{190}Os]_S$ is then used to calculate the concentration of a sample using the fractional abundance of ^{190}Os ($=f^{190}_{[^{190}Os]_S}$) in the sample and the sample weight: $[Os]_S = \frac{f^{190}_{[^{190}Os]_S}}{SampleWt.}$. For a given $(^{188}Os/^{190}Os)_M$ ratio the relative error associated with the estimated concentration from isotope dilution for a single analysis depends on ion counting and tracer weighing errors (e.g., ref. 10):

$$\frac{\Delta\left[{}^{190}Os\right]_S}{\left[{}^{190}Os\right]_S} = \frac{\Delta\left[{}^{190}Os\right]_T}{\left[{}^{190}Os\right]_T} + \frac{\Delta\left(\frac{^{188}Os}{^{190}Os}\right)_M}{0.5\times\left[\left(\frac{^{188}Os}{^{190}Os}\right)_T - \left(\frac{^{188}Os}{^{190}Os}\right)_S\right]} \times \left[\frac{1}{f_{[^{190}Os]_S}\left(1-f_{[^{190}Os]_S}\right)}\right].$$

Here the left-hand term reflects the relative error associated with the calculated abundance of ^{190}Os in the sample, the first term on the right shows the relative error associated with the weighing of the tracer, and the second term on the right gives the relative error associated with the measured ($^{188}Os/^{190}Os$) ratio multiplied by an amplification factor that depends on the fractional abundance of sample-derived ^{190}Os in the spiked sample ($=f_{[^{190}Os]_S}$); the smallest amplification factor is 4, corresponding to an $f_{[^{190}Os]_S}$ of 0.5. Because $(^{188}Os/^{190}Os)_S \sim 0.5$ and $(^{188}Os/^{190}Os)_T \sim 0$, the above equation gives an optimal $(^{188}Os/^{190}Os)_M$ ratio ($= 0.5\times\left[\left(\frac{^{188}Os}{^{190}Os}\right)_T - \left(\frac{^{188}Os}{^{190}Os}\right)_S\right]$) of ~0.25. The typical relative errors associated with tracer weighing and the measured ($^{188}Os/^{190}Os$) ratio ($= \Delta\left(\frac{^{188}Os}{^{190}Os}\right)_M / \left(\frac{^{188}Os}{^{190}Os}\right)_M$) for the samples are 2×10^{-4} and 2×10^{-3}, respectively. For an optimally spiked sample the relative error in the measured ($^{188}Os/^{190}Os$) ratio is multiplied by a factor of ~4, meaning that the second term on the right is about 40 times the first term and dominates the relative error in concentration determined by isotope dilution. The uncertainty associated with determination of Os concentration using the procedure described above is therefore of the order of 0.8% (2σ relative standard deviation). However, as can be seen from the above equations, to optimally spike a sample we need a priori to have a good idea of the concentration of the sample. Approximate Os concentration data for the bulk sediment samples were thus obtained by isotope dilution by first dissolving an aliquot of the sample. These samples were then redissolved and optimally spiked the second time. This was not possible for many of the single objects and especially the leachates that were analyzed. This resulted in larger unceratinties, when the samples were found to be either "overspiked" or "underspiked".

Procedural Blanks and Yields

For Os analyses, we obtained a procedural blank of 30 fg ($^{187}Os/^{188}Os = 0.47$) for bulk samples, 5.6 fg ($^{187}Os/^{188}Os = 0.51$) for the magnetic grains, and 2.2 fg ($^{187}Os/^{188}Os = 0.49$) for the spherule samples. The Os blank corrections are negligible (<0.1% of blank correction) because the total Os from bulk samples is >30 pg. Blank correction for magnetic grains or spherule samples is less than 2% in all cases except for the Lommel magnetic grain cluster. The blank corrections for Sr (76 pg of procedural blank), Nd (127 pg of procedural blank), and Sm (38 pg of procedural blank) are, respectively, <0.003%, <0.05%, and <0.08%, all of which are negligible. The chemical separation procedure yielded ~60% of Os, >95% of Sr, and ~90% of Nd.

1. Firestone RB, et al. (2007) Evidence for an extraterrestrial impact 12,900 years ago that contributed to the megafaunal extinctions and the Younger Dryas cooling. *Proc Natl Acad Sci USA* 104(41):16016–16021.
2. Wu Y (2011) Origin and provenance of magnetic spherules at the Younger Dryas boundary. MS thesis (Dartmouth College, Hanover, NH).
3. Bunch TE, et al. (2012) Very high-temperature impact melt products as evidence for cosmic airbursts and impacts 12,900 years ago. *Proc Natl Acad Sci USA* 109(28):E1903–E1912.
4. French HM, Demitroff M, Forman SL, Newell WL (2007) A chronology of Late-Pleistocene permafrost events in southern New Jersey, eastern USA. *Permafrost and Periglacial Processes* 18(1):49–59.

5. Chen C, Sharma M (2009) High precision and high sensitivity measurements of osmium in seawater. *Anal Chem* 81(13):5400–5406.
6. Chen C, Sharma M, Bostick BC (2006) Lithologic controls on osmium isotopes in the Rio Orinoco. *Earth Planet Sci Lett* 252(1–2):138–151.
7. Sharma M, Wasserburg GJ (1996) The neodymium isotopic compositions and rare earth patterns in highly depleted ultramafic rocks. *Geochim Cosmochim Acta* 60(22): 4537–4550.
8. Sharma M, Chen C, Blazina T (2012) Osmium contamination of seawater samples stored in polyethylene bottles. *Limnol Oceanogr Methods* 10:618–630.
9. Harvey J, Baxter EF (2009) An improved method for TIMS high precision neodymium isotope analysis of very small aliquots (1–10 ng). *Chem Geol* 258(3–4):251–257.
10. Allegre CJ (2008) *Isotope Geology* (Cambridge Univ Press, Cambridge, UK).

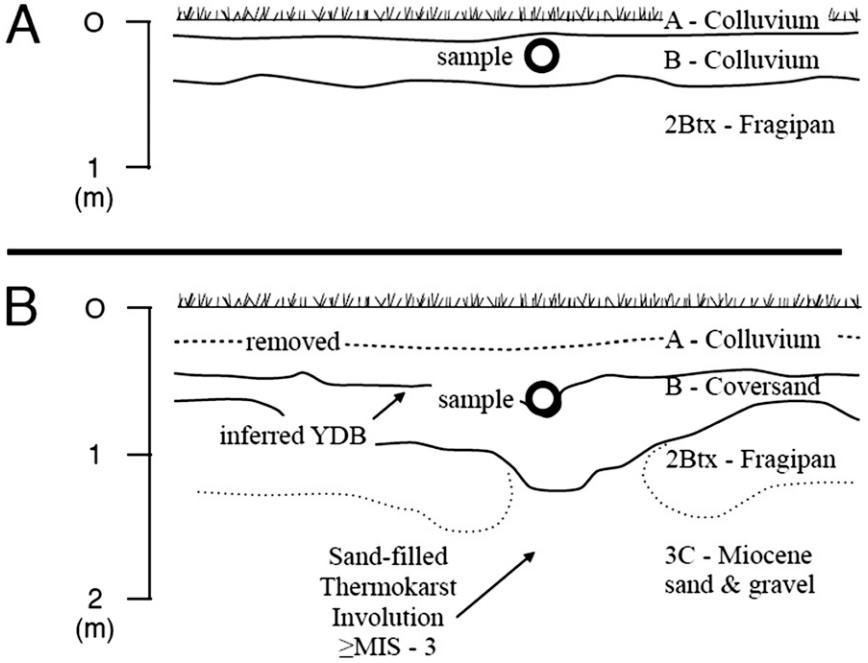

Fig. S1. (*A*) Melrose site in Pennsylvania. Colluvium ("sample") just above fragipan contained large spherules. (*B*) Newtonville site in southern New Jersey. The inferred YDB layer (a few centimeters thick) is at the contact with the black mat. A 10-cm-thick sample was taken from the bottom of the ashen-gray layer (sample).

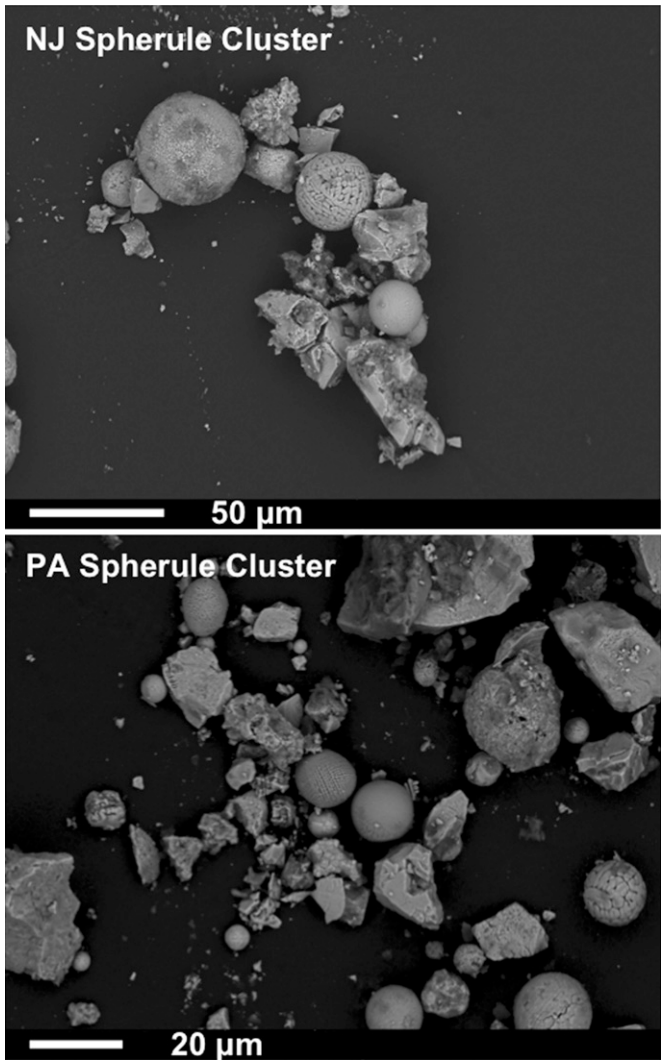

Fig. S2. SEM images of magnetic microspherules from New Jersey and Pennsylvania. Magnetic attraction creates clusters or "chains" of objects.

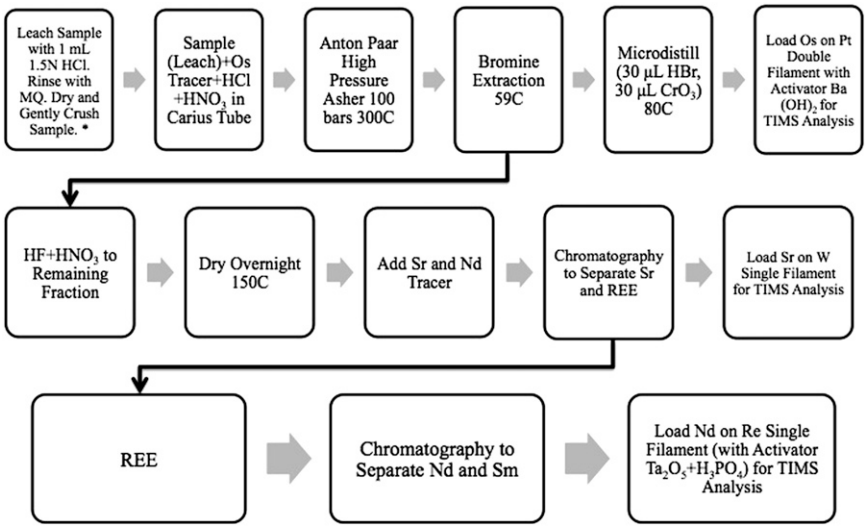

Fig. S3. Os, Sr, Nd, and Sm chemical separation procedure for spherule and bulk samples. * For bulk sample, 10 g of each sample was crushed in a zirconia ball mill and 1 g of sample was prepared for chemical separation.

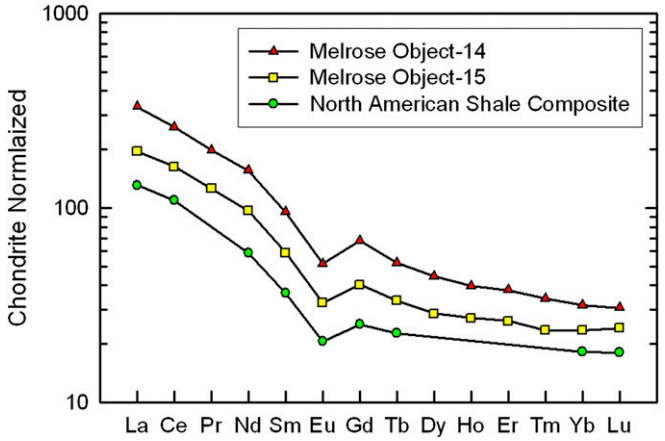

Fig. S4. Chondrite normalized REE patterns for Melrose magnetic spherules (objects 14 and 15). North American Shale Composite (NASC) data are from refs. 1 and 2.

1. Condie KC (1993) Chemical composition and evolution of the upper continental crust: Contrasting results from surface samples and shales. *Chem Geol* 104(1–4):1–37.
2. Gromet LP, Dymek RF, Haskin LA, Korotev RL (1984) The North-American Shale Composite-its compilation, major and trace-element characteristics. *Geochim Cosmochim Acta* 48(12): 2469–2482.

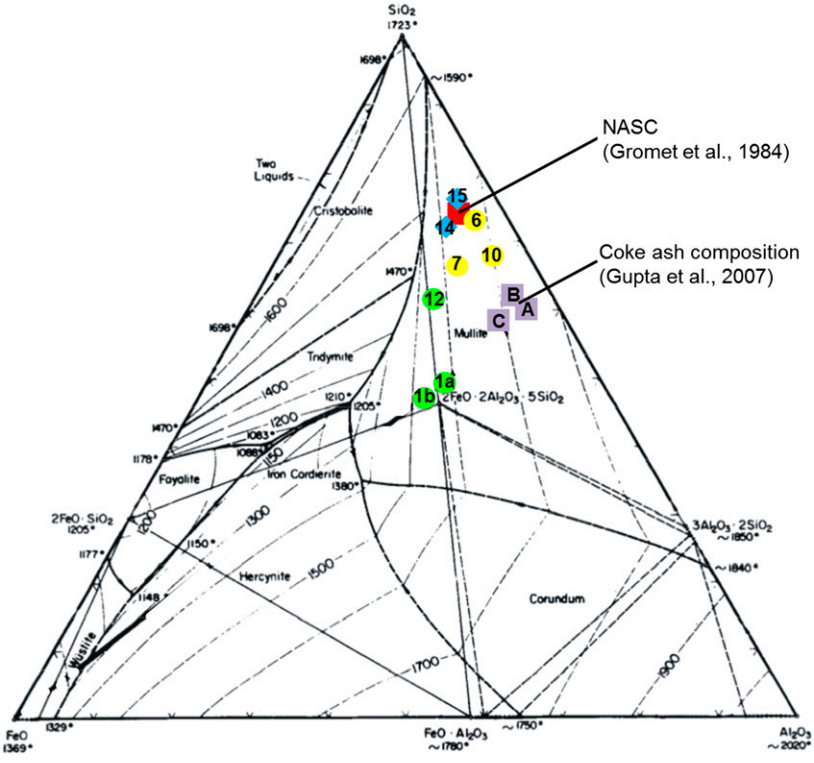

Fig. S5. SiO_2-Al_2O_3-FeO phase diagram from Huggins et al. (1). Bulk compositions of objects 14 and 15 (blue diamonds) are similar to North American Shale Composite (NASC) (2) (red square). Glass compositions of oxidized spherules (green circles) and reduced spherules (yellow circles) can be used to assess the temperature at which the glasses formed. The composition of coke ash (purple squares) from Gupta et al. (3) is shown for comparison.

1. Huggins FE, Kosmack DA, Huffman GP (1981) Correlation between ash-fusion temperatures and ternary phase-diagrams. *Fuel* 60(7):577–584.
2. Gromet LP, Dymek RF, Haskin LA, Korotev RL (1984) The North-American Shale Composite-its compilation, major and trace-element characteristics. *Geochim Cosmochim Acta* 48(12): 2469–2482.
3. Gupta S, Dubikova M, French D, Sahajwalla V (2007) Characterization of the origin and distribution of the minerals and phases in metallurgical cokes. *Energy Fuels* 21(1):303–313.

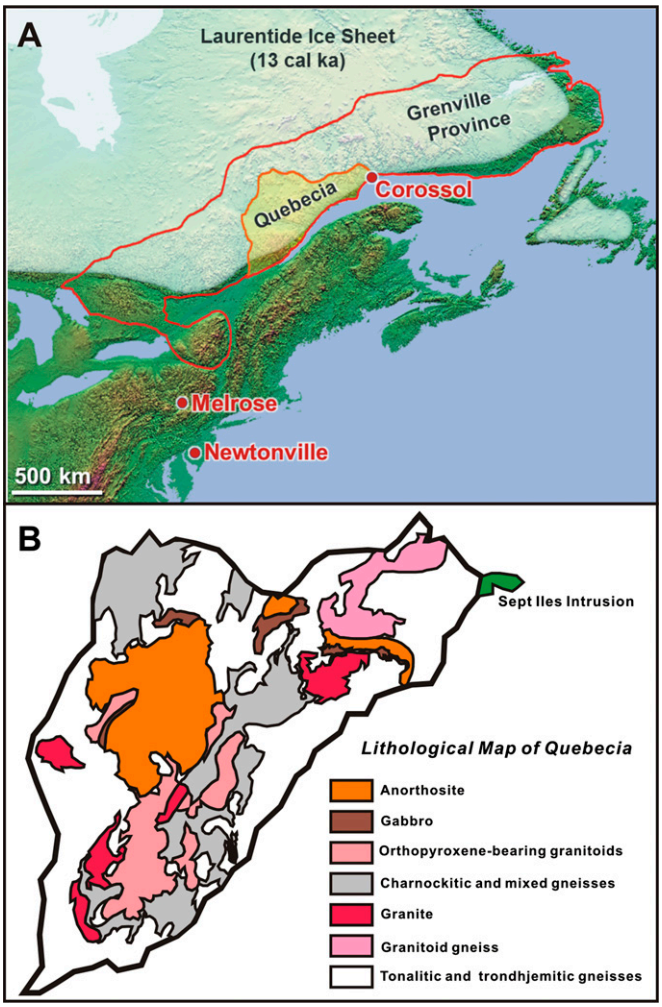

Fig. S6. (*A*) Southern extent of Laurentian Ice Sheet (1) at the time of hypothesized Corossol impact is superimposed on the outline of Grenville Province, which also contains 1.5-Ga Quebecia terrain (2–4). Positions of Corossol Crater, Melrose, and Newtonville sites are also shown. (*B*) Lithological map of Quebecia (modified from the 2012 Quebec Geological Map: www.mrn.gouv.qc.ca/english/publications/mines/map-geology-of-quebec.pdf). Note that the Quebecia terrain is a typical Grenvellian terrain with massif anothorthosites surrounded by gabbros and orthopyroxene-bearing granitoids and charnockites (hypersthene-bearing granites). Additionally, there are tonlite–trondhjemite–granite assemblages. No platinum group element (PGE)-enriched lithologies and/or ore bodies have been reported in this area (e.g., ref. 5).

1. Shaw J, et al. (2006) A conceptual model of the deglaciation of Atlantic Canada. *Quat Sci Rev* 25(17–18):2059–2081.
2. Dickin AP, Higgins MD (1992) Sm/Nd evidence for a major 1.5 Ga crust-forming event in the Central Grenville Province. *Geology* 20(2):137–140.
3. Dickin AP (2000) Crustal formation in the Grenville Province: Nd-isotope evidence. *Can J Earth Sci* 37(2):165–181.
4. Dickin AP (2010) The extent of juvenile crust in the Grenville Province: Nd isotope evidence. *Geol Soc Am Bull* 122(5/6):870–883.
5. Wilson GC (1994) Mafic-ultramafic intrusions, base-metal sulphides, and platinum group element potential of the Grenville Province in southeastern Ontario. *Ontario Geological Survey Open File Report 5880* (Ontario Geological Survey, Ontario, Canada), pp 1–296.

Table S1. Chemical composition (wt%) of microcrystals

	Mullite	Corundum	Hercynite–magnetite	Fe cordierite	Quartz
SiO_2	26.49		6.12	43.57	100.00
TiO_2	1.05		4.01	1.18	
Al_2O_3	67.14	100.00	19.69	23.13	
FeO	4.62		33.71	27.24	
Fe_2O_3			35.26		
MnO	0.01		0.01	0.04	
MgO	0.08		0.26	0.73	
CaO	0.32		0.67	1.68	
Na_2O	0.08		0.02	1.23	
K_2O	0.09			0.98	
P_2O_5	0.13			0.16	
SO_2	0.00			0.01	
NiO	0.01		0.18	0.05	
Total	100.00	100.00	100.00	100.00	100.00

Table S2. Chemical composition (wt%) of microcrystals, continued

	Native Fe	Fe sulfide phase 1	Fe sulfide phase 2	Fe silicide	Schreibersite
Fe	96.36	98.24	87.28	83.66	76.34
Ni	0.29	0.42	0.27	0.60	6.98
Co	0.54	0.38	0.29	0.21	2.14
P	0.50	0.55	0.62	0.19	11.48
Cr	0.00	0.00	0.00	0.11	0.01
Si	0.03	0.09	0.06	14.95	1.52
S	0.03	0.23	11.43	0.01	1.24
Mn	0.00	0.00	0.00	0.00	0.01
V	0.01	0.00	0.00	0.12	0.03
Ti	0.11	0.09	0.07	0.15	0.26
C	2.13				
Total	100.00	100.00	100.00	100.00	100.00

Table S3. Major element composition (wt%) and normative mineral composition (wt%) of glass and observed microcrystals in the Melrose spherules

	Object 1a	Object 1b	Object 6	Object 7	Object 10	Object 12
Major element composition						
SiO_2	46.03	43.33	67.44	58.34	62.46	53.07
TiO_2	1.21	1.33	1.34	2.68	2.02	1.52
Al_2O_3	28.86	27.13	19.71	21.62	25.74	19.81
FeO_T	18.45	21.49	4.24	8.34	3.37	12.92
MnO	0.01	0.04	0.02	0.09	0.03	0.02
MgO	0.87	1.38	0.76	1.05	1.22	0.67
CaO	2.45	3.45	1.87	1.68	0.55	8.01
Na_2O	1.18	1.02	0.93	1.12	0.33	0.00
K_2O	0.75	0.61	3.61	4.94	4.12	0.39
P_2O_5	0.20	0.18	0.06	0.03	0.12	3.55
SO_2	0.01	0.00	0.00	0.08	0.02	0.01
NiO	0.00	0.00	0.01	0.03	0.01	0.03
Total	100.00	100.00	100.00	100.00	100.00	100.00
Normative mineral composition*						
Quartz	15.79	9.06	40.71	23.02	40.88	33.74
Corundum	22.13	18.93	11.07	11.41	20.04	13.37
Orthoclase	4.43	3.63	21.32	29.33	24.35	2.33
Albite	9.96	8.66	7.92	9.51	2.81	0.00
Anorthite	10.87	16.01	8.83	8.01	1.90	16.62
Hypersthene	34.00	40.79	7.51	13.51	5.91	22.90
Ilmenite	2.31	2.52	2.54	5.11	3.81	2.84
Apatite	0.50	0.40	0.10	0.10	0.30	8.21
Observed microcrystals†						
Mullite		✓	✓	✓	✓	✓
Corundum				✓		
Hercynite						✓
Fe cordierite		✓				
Native Fe				✓		
Fe sulfide				✓		
Fe silicide					✓	
Schreibersite					✓	
Silica flow texture			✓			

*Kurt Hollocher's Excel program was used to calculate the normative mineralogy.
†Typical size of the crystals: mullite, 10–40 μm; corundum, ~20 μm; hercynite, 5–20 μm; Fe cordierite, <5 μm; native Fe, ~10 μm; Fe sulfide, <5–10 μm; Fe silicide, ~5 μm; and schreibersite, <5–10 μm.

Table S4. Bulk major element composition (wt%) and REE contents ($\mu g \cdot g^{-1}$) of two spherules collected from Melrose, PA

	Object 14*	Object 15*
SiO_2	69.6†	72.3†
TiO_2	0.77	0.93
Al_2O_3	19.3	18.5
FeO_T	7.6	4.4
MnO	0.004	0.011
MgO	0.17	0.57
CaO	0.78	0.54
Na_2O	0.93	0.32
K_2O	0.78	2.48
P_2O_5	0.00	0.00
Total	(100.00)	(100.00)
La	78.5	46.4
Ce	159.0	99.7
Pr	18.8	12.0
Nd	72.7	45.1
Sm	14.6	9.0
Eu	3.0	1.9
Gd	13.9	8.3
Tb	2.0	1.3
Dy	11.3	7.3
o	2.2	1.5
Er	6.3	4.4
Tm	0.9	0.6
Yb	5.4	4.0
Lu	0.8	0.6

*The spherules were completely dissolved using a combination of HF, $HClO_4$, and HNO_3 and the major element and REEs were measured using inductively coupled plasma optical emission spectrometry (ICP-OES) and ICP-MS, respectively.

†The SiO_2 content was estimated by subtracting from 100.00 all other major element oxides. As expected from mineral and glass compositions in Table S3, the bulk spherules are enriched in silica, alumina, and iron oxide.